Gondwana Research xxx (2012) xxx–xxx

Contents lists available at SciVerse ScienceDirect

Gondwana Research

journal homepage: www.elsevier.com/locate/gr

Tectonic evolution of the East Junggar terrane: Evidence from the Taheir tectonic window, Xinjiang, China

Xing-Wang Xu [a,b,*], Neng Jiang [a], Xian-Hua Li [a], Xun Qu [c], Yue-Heng Yang [a], Qian Mao [a], Qi Wu [a], Yong Zhang [d], Lian-Hui Dong [c]

[a] Key Laboratory of Mineral Resources, Institute of Geology and Geophysics, Chinese Academy of Sciences, Beijing 100029, China
[b] Xinjiang Research Center for Mineral Resources, Chinese Academy of Sciences, Urumqi 830011, China
[c] Xinjiang Bureau of Geology and Mineral Resources, Xinjiang, Urumqi 830000, China
[d] Tianjin Institute of Geology and Mineral Resources, China Geological Survey, Tianjin 300170, China

ARTICLE INFO

Article history:
Received 5 April 2012
Received in revised form 26 October 2012
Accepted 3 November 2012
Available online xxxx

Handling Editor: Z. Zhang

Keywords:
Tectonic evolution
East Junggar
Taheir tectonic window
Yemaquan arc

ABSTRACT

The Taheir tectonic window is located at the southern part of the Yemaquan magmatic arc in East Junggar. This paper reports detailed petrology, mineral chemistry, whole rock and Sr–Nd isotope geochemistry, hornblende $^{40}Ar/^{39}Ar$ dating, in-situ zircon U–Pb dating and Hf isotope analyses from igneous and meta-igneous rocks from this region. Our new results show that the Taheir tectonic window consists of metamorphic and deformed Ordovician volcanic rocks and granitic porphyries, Ordovician–Silurian granites and undeformed Silurian–Devonian granitic diorite, diorites and rhyolitic porphyries. The Ordovician volcanic rocks and granitic porphyries and Ordovician–Silurian granites in the Taheir tectonic window exhibit distinct features of Andean-type continental arc, such as enrichment in Pb, K and U, depletion in Nb, P and Ti, negative Eu anomalies, high La/Yb, Th/Yb and Ta/Yb values, a high proportion of dacite, rhyolite and andesite of the calc-alkaline series, massive contemporary granitic intrusions, mixtures of the juvenile material and >2.5 Ga crust, and extensive crystallization differentiation. These Ordovician volcanic rocks witnessed a series of tectonic events, including burial associated with the intrusion of 454–449 Ma granitic porphyries, underthrusting and subsidence to a depth in the middle crust associated with the intrusion of 443–432 Ma granites. The formation of albite–hornblende schists, hornblende–albite–quartz leptynites and amphibolites, the transformation from continental to continental island arc at approximately 432 Ma, the exhumation associated with the intrusion of 416–406 Ma diorites with geochemical signatures of continental island arc, and exhumation and erosion between 398 Ma and 390 Ma are also identified. The arc types that are associated with the Taheir tectonic window and its host, the Yemaquan magmatic arc, changed from Andean-type continental arc to continental island arc after the intra-arc rifting that began at 432 Ma. On the basis of the new evidence, the tectonic regime of the East Junggar terrane is redefined and a new model is proposed. It is suggested that the East Junggar terrane is related to the southward subduction of the Paleo-Asian ocean plate beneath the Junggar continent in the early Paleozoic and later shift to intra-oceanic subduction.

1. Introduction

The East Junggar terrane is one of the important tectonic units of the Central Asian Orogenic Belt (CAOB; Zonenshain et al., 1990). Debate surrounds the tectonics of the East Junggar area, including tectonic setting, age, basement nature and subduction polarity (e.g., Xiao et al., 2011; Long et al., 2012). Among the two popular models, one suggests that the Junggar is a continental block (e.g. Zhang et al., 1984, 1993; Watson et al., 1987; Xiao et al., 1992; He et al., 1994; Li et al., 2000; Charvet et al., 2001, 2007; Xu et al., 2003; Zhao et al., 2003; Buslov et al., 2004; Xu and Ma, 2004; Dong et al., 2009; Bazhenov et al., 2012; Choulet et al., 2012; Zhang et al., 2012). The other model proposes that the Junggar has a basement of Paleozoic oceanic crust (e.g., Carroll et al., 1990; Zheng et al., 2007) or oceanic island arc complexes (e.g., Coleman, 1989; Chen and Jahn, 2004; Windley et al., 2007) of the Altaid Paleozoic rocks (e.g., Sengör et al., 1993; Sengör and Natal'in, 1996; Allen and Vincent, 1997; Filippova et al., 2001; Xiao et al., 2004a, 2004b, 2008, 2009, 2010a, 2010b, 2012). The tectonics in the Eastern Junggar area are interpreted to be related to late Paleozoic intra-oceanic accretion induced by northward subduction of the Junggar oceanic lithosphere (e.g. Xiao et al., 2008, 2009; Biske and Seltmann, 2010; Wan et al., 2011; Yang et al., 2011) or by the southward subduction of the Paleo-Asian oceanic lithosphere (Zhang et al., 2004; Wong et al., 2010; Su et al., 2012).

* Corresponding author at: Key Laboratory of Mineral Resources, Institute of Geology and Geophysics, Chinese Academy of Sciences, Beijing 100029, China. Tel.: +86 10 82998198; fax: +86 10 62010846.
E-mail address: xuxw@mail.iggcas.ac.cn (X.-W. Xu).

1342-937X/$ – see front matter
http://dx.doi.org/10.1016/j.gr.2012.11.007

In this contribution, we report new data from the metamorphosed volcanic rocks and magmatic rocks from the Taheir tectonic window in the East Junggar region which is situated between the Zaisan–Erqis–the Main Mongolian Lineament-suture and the Kelameili suture and occupies the central area of the CAOB. The new results help to constrain the tectonic evolution of the Yemaquan arc and the basement and to address the evolution of East Junggar.

2. Regional tectonic setting

The Junggar terrane consists of the East and West Junggar terranes and the Junggar block and is bound by the Zaisan–Erqis—Main Mongolian Lineament/suture in the north (e.g., Chen and Jahn, 2004; Xiao et al., 2008). The Zaisan–Erqis–Main Mongolian Lineament-suture, represented by a Devonian–Carboniferous ophiolite belt (e.g., Zhang et al., 2003; Wu et al., 2006a; Kröner et al., 2007), possibly marks the final line of closure of the Paleoasian ocean between the Altaids and the Junggar terrane (Fig. 1a). The successive northward subduction of the Paleoasian ocean produced Altaids, separated by sequential ophiolites with ages of 1020 to 325 Ma, from the present margin of the Siberian craton to southern Siberia and northern Mongolia as well as to the main Mongolian Lineament in the Carboniferous (Windley et al., 2002; Kröner et al., 2007).

The East Junggar terrane to the east of the Junggar basin consists of the NW-trending Sawuer Devonian–Carboniferous oceanic island arc, the Armantai Cambrian–Ordovician ophiolite belt, the Yemaquan Paleozoic volcanic arc and the Kelameili Devonian–Carboniferous ophiolite belt from north to south (Xiao et al., 2006) (Fig. 1b).

The Sawuer oceanic island arc to the south of the Zaisan–Erqis–the Main Mongolian Lineament suture is characterized by the occurrence of Devonian adakites, porphyry Cu–Au deposits and Nb-enriched basalts (Zhang et al., 2004, 2006, 2009; Dong et al., 2009). The Armantai ophiolite belt has an age of 503–481 Ma (Jian et al., 2003; Xiao et al., 2006). The Yemaquan magmatic arc is characterized by the occurrence of the Silurian–Devonian intermediate-acid stocks and copper-bearing porphyries in the Qiongheba area (Dong et al., 2009; Qu et al., 2009; Du et al., 2010) and abundant alkaline granites associated with Sn deposits in the Kelameili area (Lin et al., 2007; Tang et al., 2007). The Kelameili ophiolites were emplaced into the Devonian–Carboniferous volcanic-sedimentary rocks between the East Junggar terrane and the Junggar block (Fig. 1b; Shu and Wang, 2003; Bu et al., 2005) and have an age of 403 to 336 Ma (Ping et al., 2005; Tang et al., 2007), which is consistent with the occurrence of *Tuvaella* fauna in both the south and north sides of the Kelameili ophiolite belt (Zhang et al., 1983; Wang and Li, 1989).

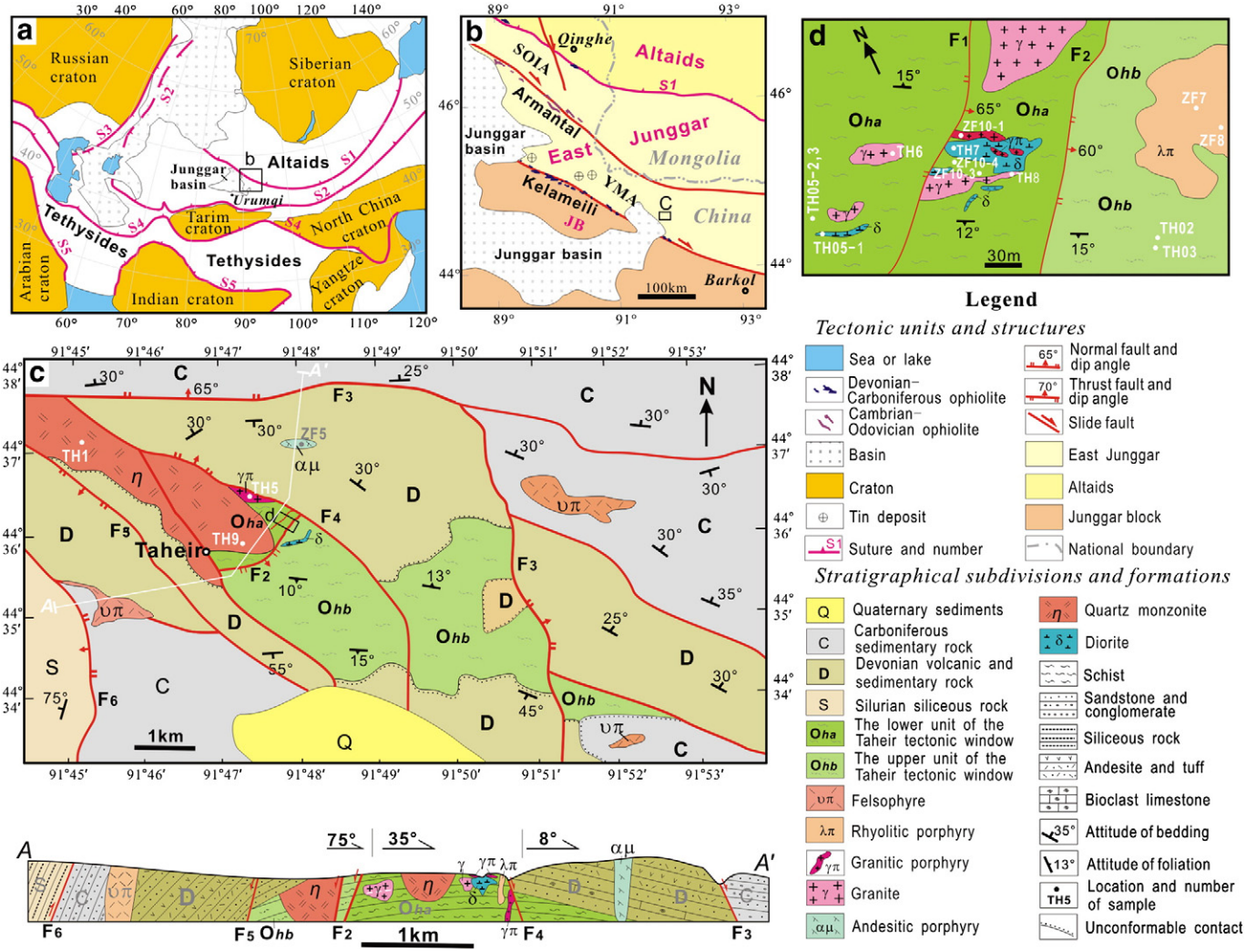

Fig. 1. Location (a) and tectonic units (b) of East Junggar and geological map (c) with an enlargement (d) of the Taheir area. Panels a and b are after Sengör and Natal'in (1996), Xiao et al. (2008, 2010) and Lehmann et al. (2010), panel c revised after RGSTXJBGMR (1978) and panel d is from the present study. JB: Junggar block, S1: Zaisan–Erqis–the Main Mongolian Lineament–Okhotsk suture, S2: Kazakhstan–Tienshan–Solonker Suture, S3: Ural suture, S4: W. Kunlun–Altyn–Qilian–Qinling–Dabie Suture, S5: Alpine–Himalayan suture, SOIA: Sawuer oceanic island arc, YMA: Yemaquan magmatic arc.

Please cite this article as: Xu, X.-W., et al., Tectonic evolution of the East Junggar terrane: Evidence from the Taheir tectonic window, Xinjiang, China, Gondwana Research (2012), http://dx.doi.org/10.1016/j.gr.2012.11.007

3. Geology of Taheir

Taheir is located at the southern part of the Yemaquan magmatic arc which is bound by the Kelameili ophiolite belt to the south and about 150 km northwest of the town of Barkol, Xinjiang, China (Fig. 1b). The rocks in the Taheir area consist of a tectonic window with some intrusive bodies, Silurian siliceous rocks, Devonian volcanic and sedimentary rocks, Carboniferous sedimentary rocks and Quaternary sediments (Fig. 1c).

The exposed rocks in the Taheir tectonic window include metamorphosed volcanic and intrusive rocks termed as Ordovician Huangcaopo Group based on regional stratigraphic correlation (RGSIXJBGMR, 1978; XBGMR, 1993). On the basis of composition and the deformation and metamorphic grade of the volcanic rocks and their associated intrusions, these rocks can be divided into two units by a NE-trending normal fault (F_2, Fig. 1c), a lower unit at the northwest and an upper unit in the middle and eastern part.

The volcanic rocks of the lower unit (O_{ha}) consist of dacite, agglomerate and breccia dacite, and volcanic block, breccia and tuff. The lower unit rocks are characterized by abundant pyroclastic lava rocks (Fig. 2a–d). Most of the block and breccia are rhyolite and dacite, with minor andesite, trachyte and trachyandesite. Plagioclase phenocrysts are common in these lavas, whereas glomerocrysts with accumulated textures and granite breccia are present in some rhyolite blocks and breccias (Fig. 2e and f). The exposed thickness of the lower unit is approximately 275 m (RGSIXJBGMR, 1978). All of these pyroclasts are intensely stretched parallel to lineations in gneisses and amphibolites, from the megascopic to the microscope scales (Fig. 2a–d), and have an average axial ratio of 6.9:2:1, corresponding to a strain k parameter of 2.45. These volcanic rocks experienced greenschist-facies to epidote–amphibolite–facies metamorphism. The fine-grained amphibolites consist of nearly equal amounts of hornblende and andesine with little magnetite and have intensive lineation that is observed by the alignment of elongate grains of hornblende (Figs. 2d and 3a). There are some

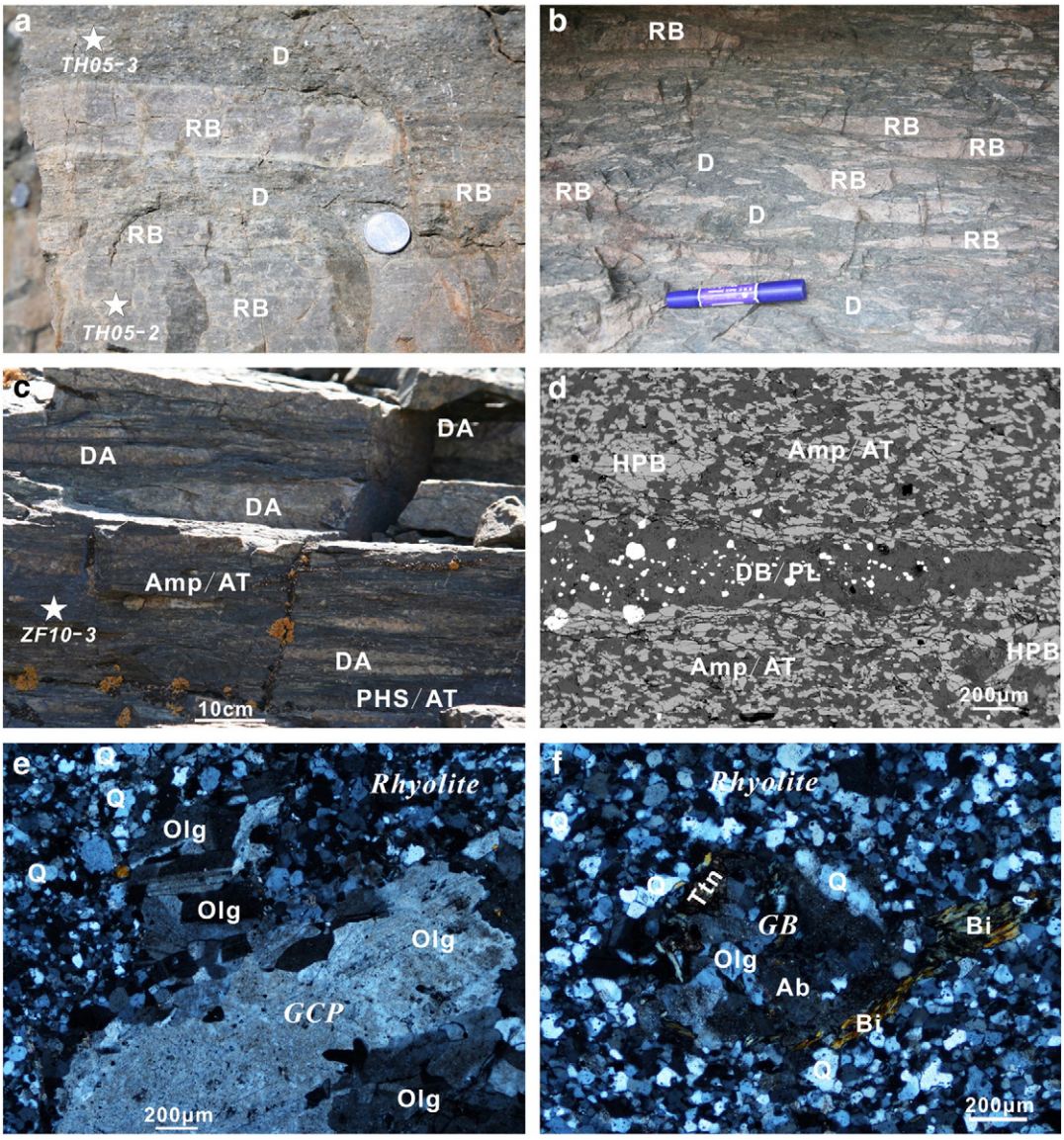

Fig. 2. Field photographs (a, b and c), back scattered electron image (d) and polarized microscopic images (e and f) showing the composition and deformation features of metamorphic volcanic rocks from the Taheir tectonic window. Image d is from a thin section of sample ZF10-3-1 collected at site ZF10-3 in image c. Both the glomerocrysts of plagioclase (GCP) with the tower-shape accumulated structure (referring after Xu et al., 2009) (image e) and granite breccia (GB) (image f) are from thin section of rhyolite block 10TH05-2 in image a. The coin in image a is 2 cm in diameter. The marker pen in image b is 14 cm long. The star and associated label in images a and c show the location and number of the collected samples. Ab: albite, Amp/AT: amphibolites from andesitic tuff, Bi: biotite, D: dacite, DA: dacite agglomerate, DB/PL: plagioclase leptynite metamorphosed from dacite breccia, HPB: hornblende porphyroblast, Olg: oligoclase, Q: quartz, RB: rhyolite block, Ttn: titanite.

Please cite this article as: Xu, X.-W., et al., Tectonic evolution of the East Junggar terrane: Evidence from the Taheir tectonic window, Xinjiang, China, Gondwana Research (2012), http://dx.doi.org/10.1016/j.gr.2012.11.007

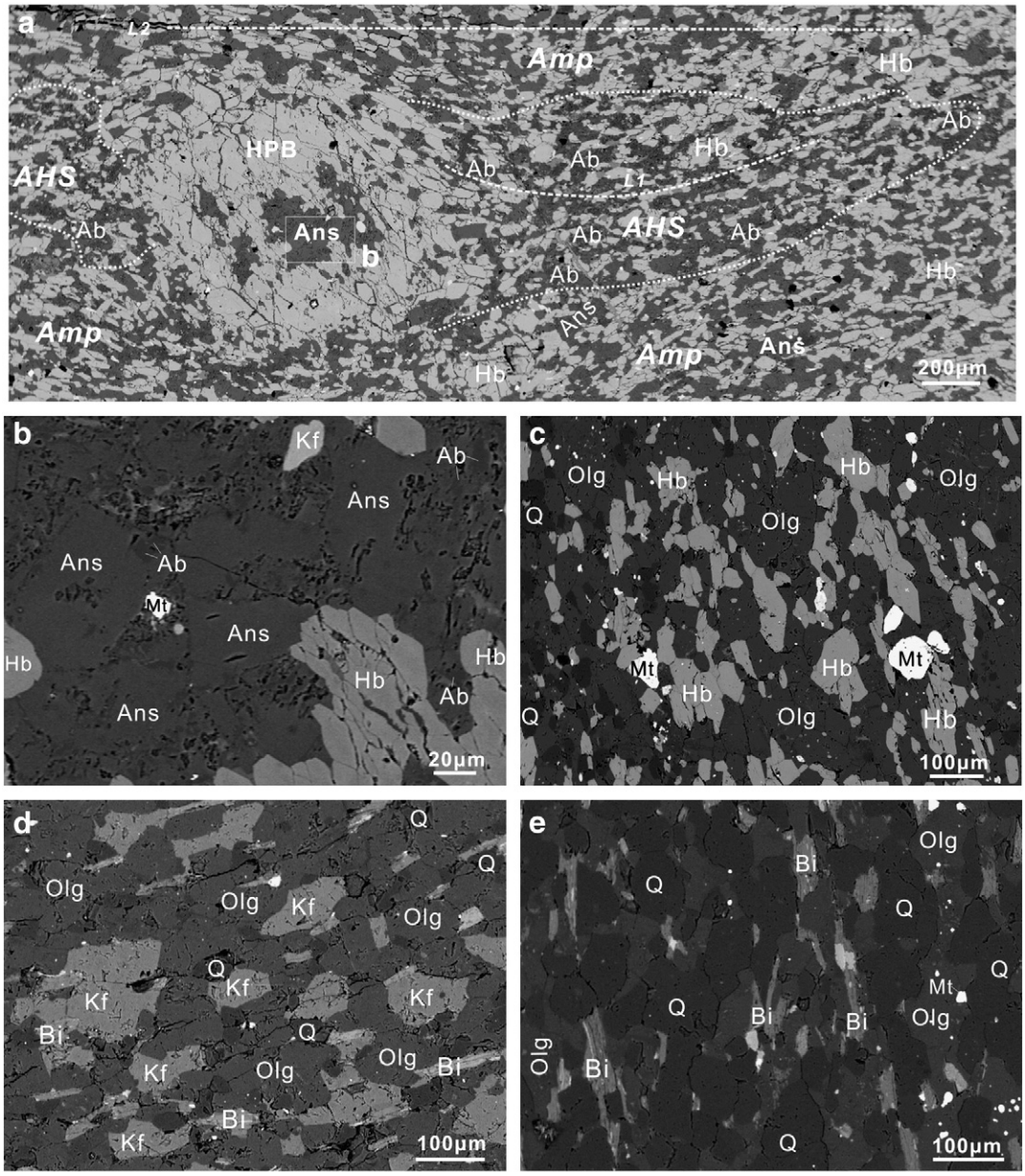

Fig. 3. Back scattered electron images showing amphibolites containing hornblende porphyroblasts and albite–hornblende schist (a) and an enlargement of intragranular andesine inclusions with relict albites (b), quartz–hornblende–oligoclase gneiss (c), biotite–quartz–K-feldspar–oligoclase gneiss (d) and biotite leptynite (e) from the lower unit of the Taheir tectonic window. Ab: albite, AHS: albite–hornblende schist, Amp: amphibolites, Bi: biotite, H: hornblende, Kf: K-feldspar, Mt: magnetite, Olg: oligoclase, Q: quartz. L_1 and L_2 are lineation in albite–hornblende schist and amphibolites, respectively.

hornblende porphyroblasts with intragranular andesine inclusions with relict albite, and some albite–hornblende schist strips in these amphibolites (Fig. 3a and b). σ-structures are presented by hornblende porphyroblasts associated with albite–hornblende schist tails on two sides (Fig. 3a). Both the σ-structures and the curved lineation in the albite–hornblende schist are bounded by straight lineations in the host amphibolite, implying that these rocks had suffered two-stage deformation. The gneiss consists of oligoclase, hornblende, K-feldspar, quartz, biotite and magnetite and has a distinctly banded structure, such as the quartz–oligoclase layer and the hornblende–oligoclase layer shown in Fig. 3c and the biotite–quartz–K-feldspar–oligoclase layer shown in Fig. 3d. The leptynites consist of granular quartz and oligoclase with minor biotite and magnetite (Fig. 3e). The grain sizes of metamorphic plagioclase are typically 50–100 μm in length. Intensive stretching lineations are NE-trending on the horizontal foliations.

In contrast, the dacite lavas and agglomerate and rhyolite blocks and breccias are weakly metamorphosed. They are characterized by the replacement of oligoclase by albite and the occurrence of hornblende, biotite, epidote, titanite and magnetite in a foliation zone. Some rhyolite blocks have a 150–200-μm-wide magnetite–albite shell, while some andesite breccias have a 200-μm-wide epidote shell. Some elongated microbreccias of dacite are metamorphosed to form andesine leptynites in amphibolites (Fig. 2d), while an augen of hornblende–albite leptynite is observed in thin section of an amphibolite specimen (ZF10-3-2). The oriented pyroclasts and the metamorphic plagioclase, hornblende and biotite formed foliation structures, which display an EW-trending gentle anticline structure (Fig. 1c and profile A–A′).

There are many foliated granite stocks and granitic porphyry dikes embedded in the metamorphic volcanic rocks of the lower unit (Fig. 1d). All of the granites and granitic porphyries experienced greenschist to epidote–amphibolite facies metamorphism and ductile deformation with foliation parallel to the schistosity in the metamorphic volcanic rocks (Fig. 4a). Network-like foliation and lenticular

Please cite this article as: Xu, X.-W., et al., Tectonic evolution of the East Junggar terrane: Evidence from the Taheir tectonic window, Xinjiang, China, Gondwana Research (2012), http://dx.doi.org/10.1016/j.gr.2012.11.007

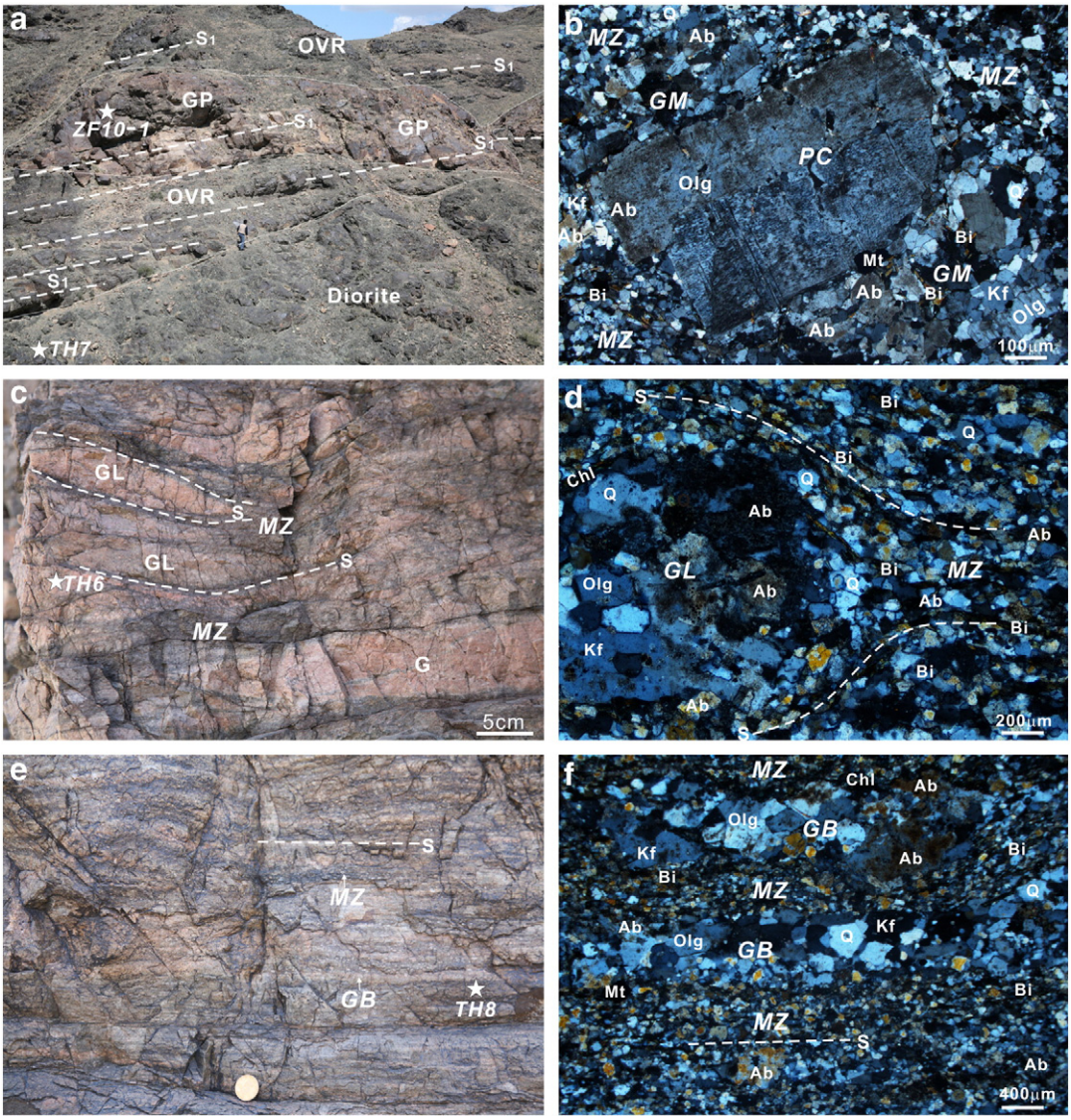

Fig. 4. Field photographs (left) and polarized microphotographs (right) of foliated granitic porphyry (a and b), generally (c and d) and intensively (e and f) foliated granites from the Taheir tectonic window. Image a shows the relationship among the Ordovician volcanic rocks (OVR), granitic porphyry (GP), schistosity (S_1) and diorite (a). Images b, d and e are taken from thin sections of sample ZF10-1, TH6 and TH8, respectively. Their locations are shown by the star in image a, c and d correspondingly. The coin in image c is 2 cm in diameter. Dashes in images show the attitude of schistosity. Ab: albite, Bi: biotite, GB: granite band, GL: granite lens, GM: groundmass, Kf: K-feldspar, MZ: mylonite zone, Mt: magnetite, Olg: oligoclase, PC: phenocryst, Q: quartz.

structures (Fig. 4c and d) are present in some moderately deformed granites, whereas banding relicts and parallel foliation zones presented by oriented biotite, chlorite, albite and quartz (Fig. 4e and f) occur in intensively deformed granites. There are some narrow epidote–hornblende–albite (epidote–amphibolite facies) mylonite zones in the intensively foliated granites. The granitic porphyries are composed of 0.5- to 3-mm-sized oligoclase, quartz and K-feldspar phenocrysts that are set in a 100- to 200-μm-sized groundmass of quartz, oligoclase and K-feldspar. However, oligoclase was partly or completely replaced by albite in intensive deformation zones. The grain size of the groundmass was reduced to 20- to 50-μm in diameter by dynamic recrystallization to form mylonite zones (Fig. 4b). The granites consist of oligoclase (50 vol.%, 400–600 μm in length), quartz (40 vol.%, 400–600 μm in diameter) and K-feldspar (10 vol.%, 400–800 μm in length). Similarly, oligoclase and K-feldspar in these foliated granites are partly or completely replaced by albite. Recrystallized quartz (20–50 μm in diameter), albite (50–100 μm in length), biotite and chlorite arrange along mylonite zones and schistosity structures, which are parallel to the schistosity in metamorphosed volcanic rocks. RGSIXJBGMR (2000) suggested that the foliated granites are of Proterozoic age, based on a $^{207}Pb/^{206}Pb$ age of 933 Ma. However, the $^{207}Pb/^{206}Pb$ age of zircon is not consistent with the $^{206}Pb/^{238}U$ and $^{207}Pb/^{235}Th$ ages of 249 Ma and 326 Ma, respectively, and this $^{207}Pb/^{206}Pb$ age (933 Ma) is not considered to represent the formation age of the analyzed granite (Hu and Wei, 2003).

Volcanic rocks of the upper unit (O_{hb}) consist mainly of trachyandesite, andesite, andesitic porphyry, agglomerate and breccia trachyandesite and andesite, and volcanic breccia and tuff. Their exposed thickness is approximately 1113 m (RGSIXJBGMR, 1978). Compared with the volcanic rocks of the lower unit (O_{ha}), the metamorphism and deformation of those in the upper unit are relatively weak and characterized by the occurrence of calcite–chlorite–albite schist interlayered with some epidote–albite–hornblende schist in intensive deformation zones adjacent to the lower unit and to fault F_2. Chloritization and albitization are present in the middle, eastern part of the Taheir tectonic window. Moreover, there are many rhyolitic porphyry dikes embedded in the volcanic rocks of the upper unit (O_{hb}). These rhyolitic porphyries also contain glomerocrysts (GC) with accumulated textures, such as the five oligoclase tablets that were packed in the GA1 and shown in Fig. 5a. These rhyolitic porphyries had suffered brittle shear deformation

Please cite this article as: Xu, X.-W., et al., Tectonic evolution of the East Junggar terrane: Evidence from the Taheir tectonic window, Xinjiang, China, Gondwana Research (2012), http://dx.doi.org/10.1016/j.gr.2012.11.007

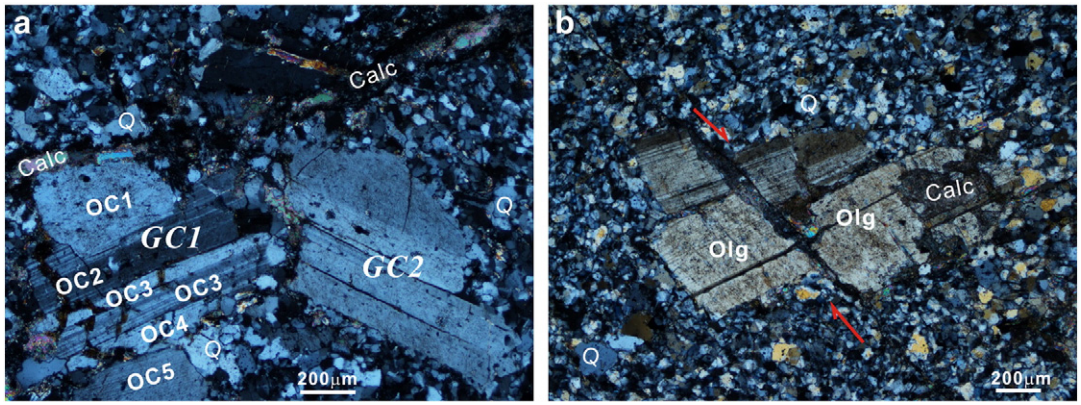

Fig. 5. Polarized microphotographs showing glomerocrysts (GC) (a) and fracture (b) in rhyolitic porphyry from the Taheir tectonic window. The images are taken from thin section of samples ZF8-2. PC1-5: plagioclase crystal 1–5. Calc: calcite, Pl: plagioclase, Q: quartz.

associated with carbonatization and weakly albitization, and some phenocrysts were broken and dislocated (Fig. 5b).

Except for granite, granitic and rhyolitic porphyries, some diorite dikes and a granodiorite stock intruded and cut the metamorphic volcanic rocks and foliated granites and granitic porphyries in the Taheir tectonic window (Figs. 1c, d and 3a). There are some dioritic porphyry inclusions in the granitic diorite stock. These granodiorite and diorites show weak albitization and chloritization.

The metamorphosed volcanic rocks with deformed granitic porphyries and granites and undeformed granitic diorites are unconformably overlain by Devonian volcanic and sedimentary rocks, which consist of limestone containing *Thamnopora* sp., *Syringaxon* sp., *Syringaxon* cf. *bakterion* and *Isorthis* sp. bioclasts in the lower part, andesite and andesitic porphyry in the middle part; and tuff in the upper part. The Carboniferous sedimentary rocks consist of conglomerates and sandstones.

Most faults within and adjacent to the Taheir tectonic window, such as F_1, F_2 and F_3 in Fig. 1c and F_5 in Fig. 1d, are detachment faults, which caused the metamorphic and deformed volcanic rocks to be exposed at the present surface. However, fault F_4 at the southwest side of the Taheir residential area is a west-dipping reverse fault, which caused the Silurian siliceous rock to thrust over the Carboniferous sandstone. Some felsophyre bodies intruded along these faults, while some felsophyre bodies embedded in Carboniferous sedimentary rocks.

4. Sample selection and analytical techniques

After petrographic examination, a total of 20 representative fresh rock samples were selected from metamorphic rocks, various lavas and intrusive bodies. A total of 18 samples were selected for whole rock geochemistry, 13 samples were selected for in situ zircon U–Pb dating and Hf isotopic analysis, 11 samples were selected for electron microprobe analysis, 14 samples were selected for Sr–Nd isotope analysis, and 2 samples were selected for $^{40}Ar/^{39}Ar$ dating. The location, rock type and analytical methods used for these samples are presented in Table 1. All analyses were conducted at the Institute of Geology and Geophysics, Chinese Academy of Sciences (IGGCAS).

For geochemical analyses, hand specimens were crushed in a tungsten carbide swing mill, sieved, ultrasonically cleaned several times in deionized water and then ground in an agate mortar. Rock powders (~1.2 g) were then dissolved with Li2B4O7 (6 g) in a TR-1000 S automatic bead fusion furnace at 1100 °C for 10 min. Major element abundances (wt.%) were determined on whole-rock powder pellets by X-ray fluorescence (XRF) using an XRF-1500 sequential spectrometer. Analytical uncertainties are 1 to 3% for major elements. Loss on ignition was obtained by weighing after 1 h of calcinations at 1100 °C. For rare earth element (REE) and trace element analyses, rock powders (50 mg) were dissolved using a mixed acid (HF:HClO4 = 3:1) in capped Savillex Teflon beakers at 120 °C for 6 days, and subsequently dried to wet salt and redissolved in 0.5 ml $HClO_4$. The solutions were then evaporated to wet salt at 140 °C and redissolved in 1 ml HNO_3 and 3 ml water for cr. 24 h at 120 °C. The solutions were diluted in 2% HNO_3 for analysis. REE and trace element concentrations were determined by inductively coupled plasma mass spectrometry (ICP-MS) using a PQ2 Turbo system. Uncertainties based on repeated analyses of internal standards are ±5% for REE and ±5–10% for trace elements.

Compositions of minerals from 16 thin sections from metamorphic and igneous rocks in the Taheir area were analyzed using a CAMECA SX51 electron microprobe at IGGCAS. The accelerating voltage was 21 kV and the sample current was 10 nA. Beam diameters ranging from 5 to 10 μm were used, depending on the contents of volatile components within the mineral being analyzed. The counting times for all elements were 10 s. Well defined natural minerals were used as standards.

Samples for isotopic analysis were dissolved in Teflon bombs after being spiked with ^{84}Sr, ^{87}Rb, ^{150}Nd and ^{147}Sm tracers prior to HF + HNO_3 (with a ratio of 2:1) dissolution. Rb, Sr, Sm and Nd were separated using conventional ion exchange procedures and measured using a Finnigan MAT 262 multi-collector mass spectrometer (Yang et al., 2004). Procedural blanks were <100 pg for Sm and Nd and <500 pg for Rb and Sr. $^{143}Nd/^{144}Nd$ were corrected for mass fractionation by normalization to $^{146}Nd/^{144}Nd = 0.7219$, and $^{87}Sr/^{86}Sr$ ratios were normalized to $^{86}Sr/^{88}Sr = 0.1194$. Typical within-run precision (2σ) for Sr and Nd was estimated to be ±0.000015. The measured values for the La Jolla and BCR-1 Nd standards and the NBS-607 Sr standard were $^{143}Nd/^{144}Nd = 0.511853 \pm 7$ ($2\sigma_n$, n = 3) and 0.512604 ± 7 ($2\sigma_n$, n = 3), respectively, and $^{87}Sr/^{86}Sr = 1.20042 \pm 2$ ($2\sigma_n$, n = 12) during the period of data acquisition (Yang et al., 2006).

Zircon grains were separated using conventional heavy fraction and magnetic techniques. Representative zircon grains, together with zircon standard 91500 were mounted in epoxy mounts which were then polished to a section of the crystals in half for analysis. More than one thousand zircon grains were separated from most samples, and about two hundred of them were mounted in a row, excepting that less than two hundred zircon grains were obtained from samples TH7, TH05-1 and ZF8 and all of them were used. All mounted zircons were documented with transmitted and reflected light micrographs as well as cathodoluminescence (CL) images to reveal their internal structures, and the mount was vacuum-coated with high-purity gold prior to secondary ion mass spectrometry (SIMS) analysis. Following the CL and other imaging, the samples were vacuum-coated with high-purity gold.

Measurements of U, Th and Pb were conducted using the Cameca IMS–1280 SIMS. U–Th–Pb ratios and absolute abundances were

Table 1
Sample location, rock type and analytical method for metamorphic and igneous rocks from the Taheir area, East Junggar.

Sample number	Location	Rock type	Analytical method					
			Major and rare element	Electron microprobe	Sr–Nd isotope	SIMS zircon U-Pb age dating	LA-ICPMS zircon Hf isotope	Ar–Ar dating
TH1	N44°36′34.6″/E91°46′28.4″	Granitic diorite	√		√			
TH5	N44°36′26.4″/E91°47′25.3″	Granitic porphyry	√		√	√	√	
TH6	N44°36′07.3″/E91°47′54.2″	Foliated Granite	√	√	√	√	√	
TH7	N44°36′07.21″/E91°47′56.9″	Diorite	√	√	√	√	√	
TH8	N44°36′05.0″/E91°48′00.2″	Foliated Granite	√	√	√	√	√	
TH9	N44°35′58.3″/E91°47′40.8″	Granitic diorite	√	√	√	√	√	
TH9-2	N44°35′58.3″/E91°47′40.8″	Dioritic porphyry inclusion	√					
TH12	N44°35′32.9″/E91°46′57.3″	Rhyolitic porphyry	√					
ZF5	N44°36′45.6″/E91°47′49.1″	Andesitic porphyry	√		√	√	√	
ZF7	N44°36′06.6″/E91°48′13.2″	Rhyolitic porphyry	√					
ZF8	N44°36′04.0″/E91°48′16.9″	Rhyolitic porphyry	√	√	√	√	√	
ZF10-1	N44°36′07.7″/E91°47′57.6″	Granitic porphyry	√	√	√	√	√	
ZF10-3	N44°36′06.2″/E91°47′57.4″	Amphibolite		√				√
ZF10-4	N44°36′07.3″/E91°47′56″	Gneiss		√				
TH02-3	N44°36′07.0″/E91°47′55.5″	Trachyandesite	√		√	√	√	
TH03-3	N44°36′03.8″/E91°47′48.5″	Trachyte agglomerate	√	√	√	√	√	
TH03-4	N44°36′03.8″/E91°47′48.5″	Trachyandesite agglomerate	√					
TH05-1	N44°36′04.5″/E91°47′46.8″	Diorite	√	√	√	√	√	√
TH05-2	N44°36′05.4″/E91°47′46.8″	Rhyolite block	√		√	√	√	
TH05-3	N44°36′05.4″/E91°47′46.8″	Dacite	√	√	√	√	√	

determined relative to the standard zircon 91500 (Wiedenbeck et al., 1995), analyses of which were interspersed with those of unknown grains, using operating and data processing procedures similar to those described by Li et al. (2009). A long-term uncertainty of 1.5% (1 RSD) for $^{206}Pb/^{238}U$ measurements of the standard zircons was propagated to the unknowns (Li et al., 2010), despite that the measured $^{206}Pb/^{238}U$ error in a specific session is generally around 1% (1 RSD) or less. Measured compositions were corrected for common Pb using non-radiogenic ^{204}Pb. Corrections are sufficiently small to be insensitive to the choice of common Pb composition, and an average of present-day crustal composition (Stacey and Kramers, 1975) is used for the common Pb assuming that the common Pb is largely surface contamination introduced during sample preparation. Uncertainties on individual analyses in data tables are reported at a 1 σ level; mean ages for pooled U/Pb (and Pb/Pb) analyses are quoted with 95% confidence interval. Data reduction was carried out using the Isoplot/Ex v. 2.49 programs (Ludwig, 2001).

In situ zircon Lu–Hf isotopic analyses were carried out using a Neptune MC-ICPMS with an ArF excimer laser ablation system. Hf isotopic analyses were obtained on the same zircon grains that were previously analyzed for U–Pb isotopes, with ablation pits of 40 μm in diameter, and a laser repetition rate of 10 Hz with 100 mJ was used. Details of the technique are described by Xu et al. (2004), Wu et al. (2006b) and Li et al. (2010). During analyses, the $^{176}Hf/^{177}Hf$ and $^{176}Lu/^{177}Hf$ ratios of standard zircon (91500) were 0.282294 ± 15 ($2\sigma_n$, n = 20) and 0.00031, similar to the commonly accepted $^{176}Hf/^{177}Hf$ ratio of 0.282284 ± 3 (1σ) measured using the solution method (Goolaerts et al., 2004; Woodhead et al., 2004).

Hornblende separates from samples ZF10-3 and TH05-1 for $^{40}Ar/^{39}Ar$ analyses were obtained by crushing the sample in a tungsten carbide swing mill, sieving and collecting crystal bigger than 200 μm, and hand-picking under a binocular microscope to be 99% pure. The hornblende separates were irradiated for 37 h at the Beijing Nuclear Research Institute Reactor. Argon extraction for incremental heating was performed on the MIR10-50 Laser Fusing and Heating System in the Laboratory of Isotope Geochronology. The purified gas fractions were analyzed on a MM5400 mass spectrometer; a number of international neutron fluence monitors (standards) have been intercalibrated (Wang et al., 2005). The procedure used for CO_2 laser fusion on MM5400 of the IGGCAS follows Wang et al. (2006). Age calculations were made using decay constants given by Steiger and Jäger (1977) and formulas of Wang et al. (1985) and Wang (1992).

5. Analytical results

5.1. Whole rock geochemistry

Major and trace element data from the analyzed samples of the Taheir area are summarized in Table 2. The 5 metamorphic lava samples have a large range in major element concentrations, with SiO_2 of 52.54–79.26 wt.%, Al_2O_3 of 11.37–15.23 wt.%, Fe_2O_3 of 1.21–4.6 wt.%, FeO of 1.01–4.36 wt.%, MgO of 0.9–4.69 wt.%, CaO of 1.13–7.04 wt.%, Na_2O of 3.41–6.39 wt.%, and K_2O of 0.42–3.36 wt.%. However, they have similar trace element concentrations and ratios, with REE of 114–160 ppm, $(La/Yb)_N$ of 7.13–8.43 and Eu/Eu* of 0.74–0.87, low Rb (5.65–26.87 ppm), Nb (3.46–5.13 ppm), Y (16.35–21.01 ppm), Ta (0.2–0.31 ppm), Yb (1.81–2.49 ppm) and Ce/Pb (5.54–13.41), and high Ba/Nb (29–338), La/Yb (10.58–12.51) and Th/Yb (2.73–3.68) (Table 2). These lavas plot in the fields of rhyolite, dacite, trachyte and trachy-andesite in a total alkali versus silica (TAS) diagram (Fig. 6a) and are calc-alkaline (Fig. 6b). They have similar REE pattern with pronounced negative Eu anomalies (Fig. 7a) and are enriched in Pb and U and depleted in Nb, P and Ti in trace element spider diagrams (Fig. 7b). These rocks plot in the field of volcanic arc granites (VAG) in the Rb versus Ta + Yb diagram (Fig. 8a; Pearce et al., 1984), in the continental crust field in the Ce/Pb versus Ce diagram (Fig. 8b; Hofmann, 1988), in and near the field of arc volcanic rocks in the Ba/Nb versus La/Nb diagram (Fig. 8c; Jahn et al., 1999), in the field of continental arc in the Th/Yb versus Ta/Yb diagram (Fig. 8d; Pearce, 1983), and in interspace between the field of Andean-type continental arc and that of continental island arc in La/Yb versus Sc/Ni diagram (Fig. 8e; Bailey, 1981).

Compared with the metamorphic lava samples, the granite and granitic and rhyolitic porphyry samples have a more restricted range in major element, with SiO_2 of 70.07–76.02 wt.%, Al_2O_3 of 11.28–14.06 wt.%, Fe_2O_3 of 0.68–2.53 wt.%, FeO of 0.29–1.29 wt.%, MgO of 0.38–2.05 wt.%, CaO of 0.85–4.21 wt.%, Na_2O of 2.84–5.5 wt.%, and K_2O of 0.6–3.71 wt.%. They also have similar trace element concentrations and ratios, with REE of 85–175 ppm, $(La/Yb)_N$ of 5.69–11.99 and Eu/Eu* of 0.62–0.81, low Rb (6.7–48.16 ppm), Nb (3.78–5.81 ppm), Y (14.44–25.44 ppm), Ta (0.22–0.49 ppm), Yb (1.6–2.8 ppm) and Ce/Pb (6.08–12.28), and high Ba/Nb (26–229) and Th/Yb (2.03–5.95) (Table 2). These rocks plot in the field of granite (rhyolite) in the TAS diagram (Fig. 6a) and are calc-alkaline (Fig. 6b). They have similar REE and trace element patterns (Fig. 7) and plot in the same fields in the Rb versus

Please cite this article as: Xu, X.-W., et al., Tectonic evolution of the East Junggar terrane: Evidence from the Taheir tectonic window, Xinjiang, China, Gondwana Research (2012), http://dx.doi.org/10.1016/j.gr.2012.11.007

Table 2
Major (wt.%) and trace element (ppm) concentrations for igneous rocks from the Taheir area, East Junggar.

Sample	TH02-3	TH03-3	TH03-4	TH05-2	TH05-3	TH5	TH6	TH8	ZF10-1	ZF7	ZF8	TH12	TH1	TH9	TH9-2	TH7	TH05-1	ZF5
SiO_2	56.94	60.09	52.54	69.26	66.83	74.64	76.02	70.07	71	72.42	73.89	70.13	65.9	62.32	52.65	51.38	49.98	57.76
TiO_2	0.55	0.45	0.53	0.36	0.48	0.31	0.33	0.52	0.48	0.45	0.38	0.63	0.28	0.45	0.67	1.67	1.68	1.43
Al_2O_3	15.08	15.23	13.18	11.37	14.3	12.82	11.91	12.28	13.91	14.06	11.28	12.19	17.21	16.31	19.04	14.94	14.98	14.86
Fe_2O_3	4.6	1.21	4.46	1.24	3.01	1.36	0.79	1.98	1.72	1.36	0.68	2.53	1.26	2.44	4.21	6.59	5.94	4.41
FeO	3.83	1.01	4.36	1.08	2.08	0.86	1.49	1.92	1.24	1.67	0.71	0.29	1.37	2.57	4.39	7.11	7.38	4.62
MnO	0.13	0.06	0.16	0.04	0.1	0.05	0.05	0.08	0.05	0.03	0.05	0.14	0.07	0.09	0.15	0.22	0.22	0.2
MgO	4.69	1.15	5.08	0.9	2.49	0.38	1.03	1.21	0.68	1.07	0.46	2.05	0.83	2.49	4.68	4.69	5.57	3.57
CaO	5.43	6.32	7.04	1.13	2.91	1.87	0.85	1.54	1.79	2.89	4.25	4.21	6.97	5.24	6.69	8.16	8.48	5.72
Na_2O	5.5	6.39	5.71	3.41	5.95	3.55	4.51	4.92	5.5	2.84	3.09	2.97	2.19	2.76	2.06	2.59	2.82	2.27
K_2O	1.2	2.75	0.42	3.36	0.62	1.92	1.68	3.71	2.41	1.63	0.6	1.95	1.8	2.09	1.35	1.1	1.21	1.33
P_2O_5	0.15	0.11	0.12	0.1	0.13	0.05	0.07	0.15	0.13	0.13	0.1	0.13	0.12	0.16	0.24	0.3	0.21	0.26
LOI	1.62	5.26	3.46	8.26	1.04	2.83	1.18	1.65	1.08	1.57	3.73	1.84	1.92	2.9	3.9	1.37	0.88	3.18
TOTAL	99.72	100.03	97.06	100.51	99.94	100.65	99.9	100.02	99.99	100.11	100.23	100.06	99.91	99.82	100.03	100.12	99.35	99.62
Li	9.3	5.19	8.78	6.21	7.46	1.61	1.39	7.07	3.6	2.12	2.02	7.08	1.12	16.15	30.95	9.84	10.69	22.03
Be	0.75	0.49	0.58	0.78	1.08	0.68	1.01	1.3	1.17	1.16	0.72	0.93	0.92	0.9	1.2	0.62	0.77	0.92
Sc	23.52	9.25	23.81	8.96	17.78	3.7	4.91	12.25	9.09	9.48	4.87	1.67	3.45	9.46	20.51	37.99	39.76	29.06
V	193.74	51.28	200.14	39.95	108.49	26.24	24.94	48.7	40.38	33.54	14.57	6.32	47.44	95.27	190.8	425.52	304.3	210.67
Cr	399.08	5.49	100.93	9.37	58.53	59.49	108.34	62.97	0.5	1.64	0.94	50.39	54.65	67.28	38.98	38.61	40.14	17.91
Co	23.59	5.23	27.98	6.11	15.81	2.25	3.18	4.86	3.59	2.33	1.56	0.64	3.95	11.37	21.94	31.15	40.42	17.62
Ni	61.39	4.11	61.21	3.2	15.41	8.84	2.87	21.67	20.84	2.72	1.65	1.25	1.63	7.2	15.97	16.01	23.4	8.46
Cu	21.08	31.18	53	11.64	49.76	10.24	1.3	1.2	12.93	2.12	3.99	0.82	1.78	15.99	231.06	122.95	370.2	30.98
Zn	70.78	35.12	73.6	36.88	55.79	48.35	46.06	48.28	58.37	71.56	26.07	21.35	53.54	61.49	85.59	120.28	176.5	105.4
Ga	14.86	9.57	13.97	11.44	16.29	12.68	11.8	15.67	13.79	15.5	10.27	12.63	17	16.25	23.01	17.92	20.54	18.13
Rb	20.66	26.87	5.65	27.42	7.21	17.56	20.11	48.16	17.01	18.67	6.7	24.35	27.92	32.31	22.93	18.93	19.95	19.95
Sr	548.44	143.75	279.86	245.34	312.61	78.82	210.5	444.43	144.93	122.52	109.43	107.37	551.92	689.25	768.69	528.47	628.23	486.26
Y	16.35	21.01	17.15	19.67	20.97	14.44	17.64	25.44	21.28	23.23	19.14	17.49	8.75	12.3	16.27	28.34	34.92	28.96
Zr	144.72	204.32	133.26	194.82	181.76	191.83	197.31	214.47	201.51	169.43	137.43	104.84	94.67	100.73	61.53	85.06	129.76	115.48
Nb	3.57	5.13	3.46	4.68	4.58	4.8	4.15	5.12	4.84	4.46	3.78	5.81	2.31	2.21	2.21	3.09	2.75	3.98
Cs	0.31	0.09	0.11	0.14	0.13	0.2	0.17	0.63	0.07	0.34	0.21	0.25	0.38	0.58	0.41	0.28	0.39	0.25
Ba	436.61	671.85	99.69	1580.63	138.89	243.37	407.98	1173.2	791.98	152.02	143.75	149.15	774.41	546.18	393.57	169.27	363.32	480.32
La	20.33	31.14	23.76	28.06	25.5	28.45	25.33	35.33	31.43	27.68	17.73	17.06	9.25	12.16	15.05	7.33	10.27	11.57
Ce	43.65	63.31	45.73	58.47	53.76	59.33	54.93	70.24	65.54	60.55	41.34	32.69	20.86	24.66	33.12	18.24	24.44	27.32
Pr	6.14	8.36	6.05	7.54	7.2	6.38	6.55	9.09	8.19	7.72	5.19	3.37	2.58	3	4.46	2.78	3.89	3.88
Nd	24.29	32.42	25.1	28.71	30	22.78	26.13	34.15	32.2	30.9	20.44	19.47	10.1	12.11	18.16	13.09	18.9	17.75
Sm	5.12	6.27	5	5.62	5.83	3.75	4.84	6.65	5.97	6.4	4.41	3.92	2.02	2.62	3.9	4.11	5.55	5.23
Eu	1.29	1.37	1.29	1.28	1.29	0.74	1.03	1.54	1.48	1.48	1	0.52	0.67	0.8	1.07	1.44	1.83	1.74
Gd	4.46	5.29	4.15	4.85	4.81	3.09	3.99	5.66	5.19	4.9	3.83	1.69	1.65	2.31	3.19	4.51	5.88	4.65
Tb	0.63	0.76	0.61	0.68	0.71	0.44	0.58	0.83	0.74	0.79	0.57	0.23	0.25	0.36	0.49	0.78	1.08	0.81
Dy	3.45	4.13	3.4	3.73	3.93	2.5	3.3	4.71	4.11	4.55	3.34	3.26	1.47	2.14	3.03	5.2	6.95	5.38
Ho	0.67	0.86	0.7	0.78	0.82	0.51	0.69	0.94	0.85	0.96	0.72	0.25	0.3	0.45	0.62	1.1	1.49	1.15
Er	1.89	2.39	1.91	2.24	2.3	1.5	1.94	2.6	2.37	2.72	2.04	0.72	0.85	1.27	1.79	3.07	4.22	3.25
Tm	0.28	0.37	0.29	0.36	0.36	0.23	0.3	0.4	0.35	0.41	0.31	0.11	0.13	0.19	0.28	0.46	0.61	0.49
Yb	1.81	2.49	1.95	2.37	2.41	1.6	1.98	2.62	2.27	2.8	2.1	1.7	0.87	1.24	1.8	2.93	3.86	3.16
Lu	0.3	0.39	0.31	0.39	0.39	0.29	0.32	0.4	0.36	0.43	0.32	0.31	0.14	0.2	0.28	0.44	0.6	0.47
Hf	4.24	6.04	3.94	5.68	5.29	5.78	5.88	6.46	5.91	4.89	3.88	3.2	2.69	2.9	1.94	2.57	3.9	3.15
Ta	0.22	0.31	0.2	0.28	0.27	0.31	0.24	0.31	0.27	0.27	0.22	0.49	0.16	0.13	0.09	0.2	0.19	0.25
Tl	0.09	0.13	0.05	0.13	0.06	0.1	0.09	0.17	0.08	0.08	0.06	0.12	0.1	0.13	0.1	0.09	0.09	0.09
Pb	3.25	11.42	5.41	8.97	6.03	9.76	3.97	7.49	10.34	4.93	4.98	4.93	4.65	2.64	2.88	2.15	4.51	5.4
Bi	0.05	0.05	0.04	0.05	0.12	0.24	0.03	0.1	0.08	0.08	0.05	0.06	0.02	0.02	0.1	0.02	0.3	0.06
Th	5.98	9.16	5.32	8.11	7.67	9.52	8.05	8.88	7.58	5.99	4.27	5.25	1.45	2.19	0.47	0.58	1.38	1.38
U	1.91	2.61	1.43	2.36	2.3	3.06	1.78	2.62	2.18	1.67	1.29	1.07	0.72	1.1	1.09	0.4	0.87	0.47
REE	114.31	159.55	120.25	145.08	139.31	131.59	131.91	175.16	161.05	152.29	103.34	85.3	51.14	63.51	87.24	65.48	89.57	86.85
Eu/Eu*	0.83	0.73	0.87	0.75	0.74	0.66	0.72	0.77	0.81	0.81	0.74	0.62	1.12	0.99	0.93	1.02	0.98	1.08
LaN/YbN	7.57	8.43	8.21	7.98	7.13	11.99	8.62	9.09	9.33	6.66	5.69	6.77	7.17	6.61	5.64	1.69	1.79	2.47
Ce/Pb	13.41	5.54	8.46	6.52	8.92	6.08	13.84	9.38	6.34	12.28	8.31	6.63	4.48	9.34	11.49	8.48	5.42	5.06
Ba/Nb	122	131	29	338	30	51	98	229	164	34	38	26	335	247	178	55	132	121
La/Nb	5.69	6.07	6.87	6.00	5.57	5.93	6.10	6.90	6.49	6.21	4.69	2.94	4.00	5.50	6.81	2.37	3.73	2.91
Th/Yb	3.30	3.68	2.73	3.42	3.18	5.95	4.07	3.39	3.34	2.14	2.03	3.09	1.67	1.77	0.26	0.20	0.36	0.44
Ta/Yb	0.12	0.12	0.10	0.12	0.11	0.19	0.12	0.12	0.12	0.10	0.10	0.29	0.18	0.10	0.05	0.07	0.05	0.08
Sr/Y	33.54	6.84	16.32	12.47	14.91	5.46	11.93	17.47	6.81	5.27	5.72	14.34	63.11	56.02	47.24	18.65	17.99	16.79
Sc/Ni	0.38	2.25	0.39	2.80	1.15	0.42	1.71	0.57	0.44	3.49	2.95	1.34	2.12	1.31	1.28	2.37	1.70	3.43
La/Yb	11.23	12.51	12.18	11.84	10.58	17.78	12.79	13.48	13.85	9.89	8.44	10.04	10.63	9.81	8.36	2.50	2.66	3.66

Ta + Yb diagram (Fig. 8a), Ce/Pb versus Ce diagram (Fig. 8b), Ba/Nb versus La/Nb diagram (Fig. 8c) and Th/Yb versus Ta/Yb diagram (Fig. 8d) as the metamorphic lavas. However, the granites and granitic porphyries have higher La/Yb (12.79–17.78) and plot in or near the field of Andean-type continental arc, whereas the rhyolitic porphyries plot in the field of continental island arc in the La/Yb versus Sc/Ni diagram (Fig. 8e).

The granodiorite and dioritic porphyry samples have similar major and trace element contents, with SiO_2 of 52.65–65.9 wt.%, Al_2O_3 of 16.31–19.04 wt.%, Fe_2O_3 of 1.26–4.21 wt.%, FeO of 1.37–4.39 wt.%, MgO of 0.83–4.68 wt.% and TiO_2 of 0.28–0.67 wt.%, CaO of 5.24–6.97 wt.%, Na_2O of 2.06–2.76 wt.%, K_2O of 1.35–2.09 wt.%, P_2O_5 of 0.12–0.24 wt.%, REE of 51–87 ppm, $(La/Yb)_N$ of 5.64–7.17 and Eu/Eu* of 0.93–1.12, and relatively low Rb (22.93–32.31 ppm), Nb (2.21–2.31 ppm), Y (8.75–16.27 ppm), Ta (0.09–0.16 ppm), Yb (0.87–1.24 ppm) and Ce/Pb (4.48–11.49), and high Sr (552–769 ppm), Sr/Y (47–63) and Ba/Nb (178–335) (Table 2). These rocks are calc-alkaline (Fig. 6b) and adakitic (Defant and Drummond, 1990), and have similar REE patterns (Fig. 7a). Trace element spider diagrams indicate that they are enrichment of Pb, U and Sr and depletion of Nb, P and Ti (Fig. 7b). They plot

Please cite this article as: Xu, X.-W., et al., Tectonic evolution of the East Junggar terrane: Evidence from the Taheir tectonic window, Xinjiang, China, Gondwana Research (2012), http://dx.doi.org/10.1016/j.gr.2012.11.007

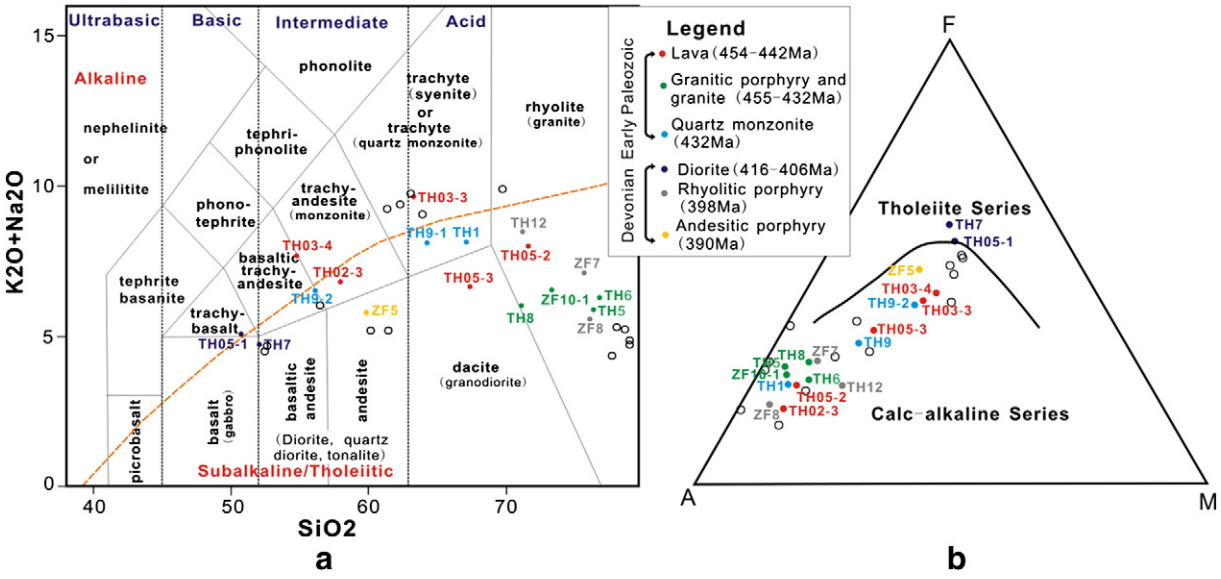

Fig. 6. TAS diagram (after Le Bas et al., 1986) (a) and AFM (after Irvine and Baragar, 1971) (b) of igneous rocks from the Taheir area. The black circles show plots of lava micro breccias, schists, leptynites, gneisses and amphibolites, whose compositions are estimated by the mineral composition and content reported in Supplementary table 1.

in the same fields in the Rb versus Ta + Yb diagram (Fig. 8a), Ce/Pb versus Ce diagram (Fig. 8b) and Ba/Nb versus La/Nb diagram (Fig. 8c) with metamorphic felsic lava, granites, and granitic and rhyolitic porphyries. However, two granodiorite samples plot in the field of continental arc, while the dioritic porphyry sample plots in interspace between the field of oceanic island arc (OIA) and that of within plate basalts (WPB) in the Th/Yb versus Ta/Yb diagram (Fig. 8d). Moreover, all the three granitic diorite and dioritic porphyry samples plot in the field of continental island arc in the La/Yb versus Sc/Ni diagram (Fig. 8e).

Two diorite samples and one andesitic porphyry have similar major and trace element contents: SiO_2 (49.98–57.76 wt.%), Al_2O_3 (14.86–14.98 wt.%), Fe_2O_3 (4.41–6.59 wt.%), FeO (4.62–7.38 wt.%), MgO (3.57–5.57 wt.%) and TiO_2 (1.43–1.68 wt.%), CaO (5.72–8.48 wt.%), Na_2O (2.27–2.82 wt.%), K_2O (1.1–1.33 wt.%), P_2O_5 (0.21–0.3 wt.%), REE (65–90 ppm), $(La/Yb)_N$ (1.69–2.74) and Eu/Eu^* (0.98–1.08), low Rb (18.93–19.95 ppm), Nb (2.75–3.98 ppm), Y (28.34–34.42 ppm), Ta (0.19–0.25 ppm), Yb (2.93–3.86 ppm) and Ce/Pb (5.42–8.46), and high Sr (486–628 ppm) and Ba/Nb (55–132) (Table 2). These rocks have similar flat REE patterns (Fig. 7a) and trace element spider

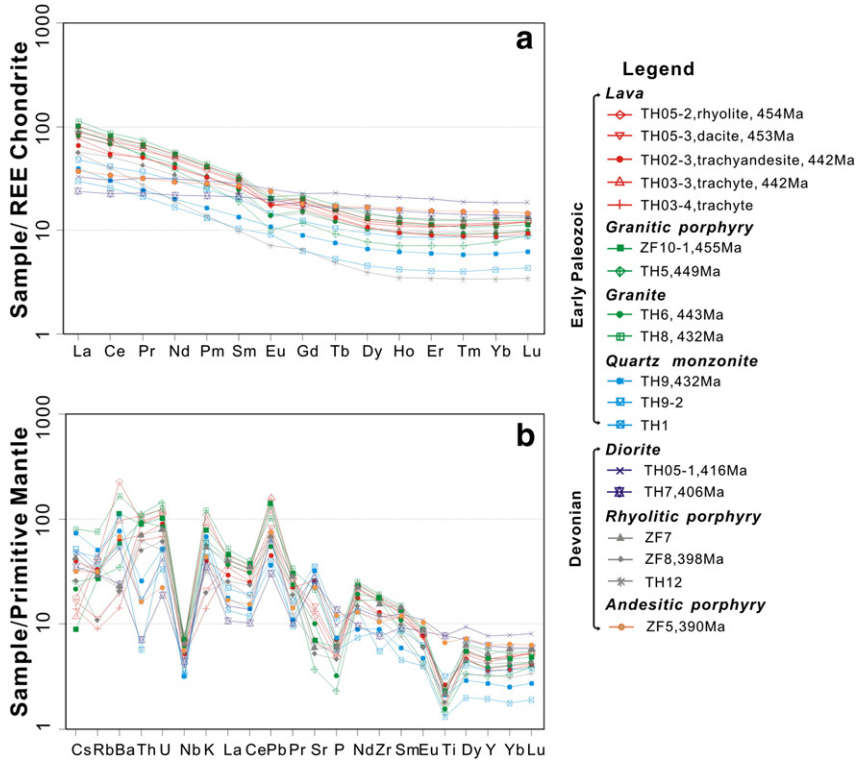

Fig. 7. REE (a) and trace element (b) spider diagrams of igneous rocks from the Taheir area. The REE and primitive mantle values are after Boynton (1984) and Sun and McDonough (1989), respectively.

Please cite this article as: Xu, X.-W., et al., Tectonic evolution of the East Junggar terrane: Evidence from the Taheir tectonic window, Xinjiang, China, Gondwana Research (2012), http://dx.doi.org/10.1016/j.gr.2012.11.007

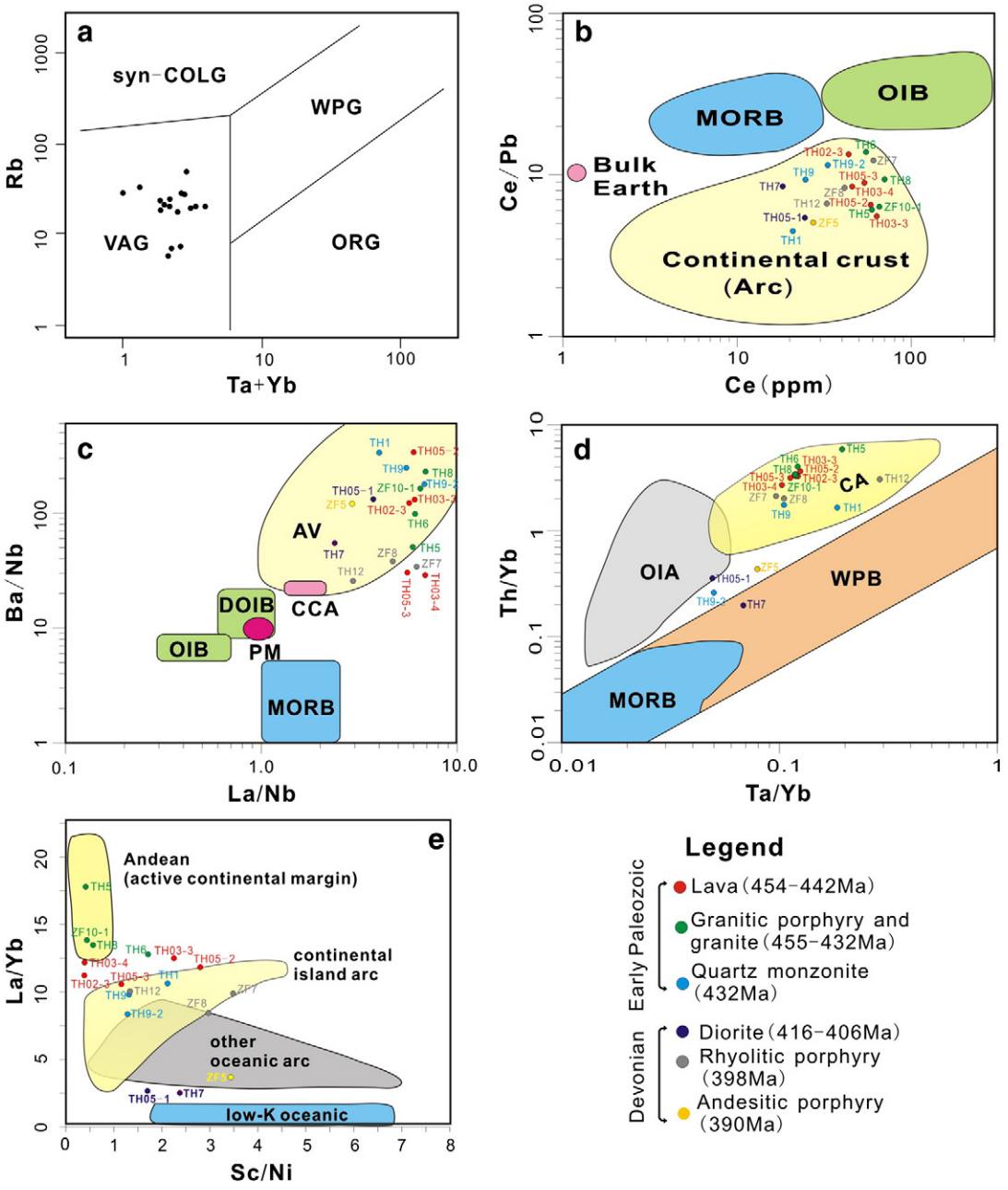

Fig. 8. (a) Rb versus Ta + Yb diagram (after Pearce et al., 1984), (b) Ce/Pb versus Ce diagram (after Hofmann, 1988), (c) Ba/Nb versus La/Nb diagram (after Jahn et al., 1999), (d) Th/Yb versus Ta/Yb diagram (after Pearce, 1983) and (e) La/Yb versus Sc/Ni diagram (Bailey, 1981) for igneous rocks from the Taheir area. AV: arc volcanics, CA: continental arc, CCA: continental crust average, DOIB: Dupal oceanic island basalt, OIA: oceanic island arc, MORB: midocean ridge basalts, OIB: oceanic island basalt, ORG: ocean ridge granites, PM: primitive mantle, syn-COLG: syn-collision granites, VAG: volcanic arc granites, WPB: within plate basalts, WPG: within plate granites.

diagrams indicate that they are enriched with Pb and Sr and depleted of Th, Nb, Pr and Zr (Fig. 7b). They plot in the same fields in the Rb versus Ta + Yb diagram (Fig. 8a), the Ce/Pb versus Ce diagram (Fig. 8b) and the Ba/Nb versus La/Nb diagram (Fig. 8c) with metamorphic felsic lava, granitic and rhyolitic porphyries, and granitic diorite and dioritic porphyry. However, these rocks all plot in or near the field of other oceanic arc in the La/Yb versus Sc/Ni diagram (Fig. 8e), and in between the continental arc (CA), oceanic island arc (OIA) and within plate basalts (WPB) fields in the Th/Yb versus Ta/Yb diagram (Fig. 8d). The diorite samples contain high Fe and Mg, and belong to the tholeiite series (Fig. 6b).

5.2. Mineral chemistry and protolith composition

Electron microprobe analyses were performed on hornblende, plagioclase, K-feldspar, biotite and chlorite from 16 thin sections from various metamorphic rocks and intrusive bodies in the Taheir tectonic window. Mineral compositions are used to constrain the classification of metamorphic rocks and to estimate the composition of micro-lava breccias and the protolithic composition of some schists, gneisses, leptynites and amphibolites.

5.2.1. Mineral chemistry

Plagioclases from granites, granitic and rhyolitic porphyries, rhyolite and dacite are albite and oligoclase with anorthite content up to 18%, while andesine from diorite and granitic diorite has an anorthite content of 30–34% (Fig. 9a). The composition of metamorphic plagioclase varies regularly with the grade of the metamorphic rocks. Albite is the major feldspars in the schists, while oligoclase is dominant in the gneisses and andesine in the amphibolites (Fig. 9a). The oligoclase from the gneisses has an anorthite content of 10–22%, and the

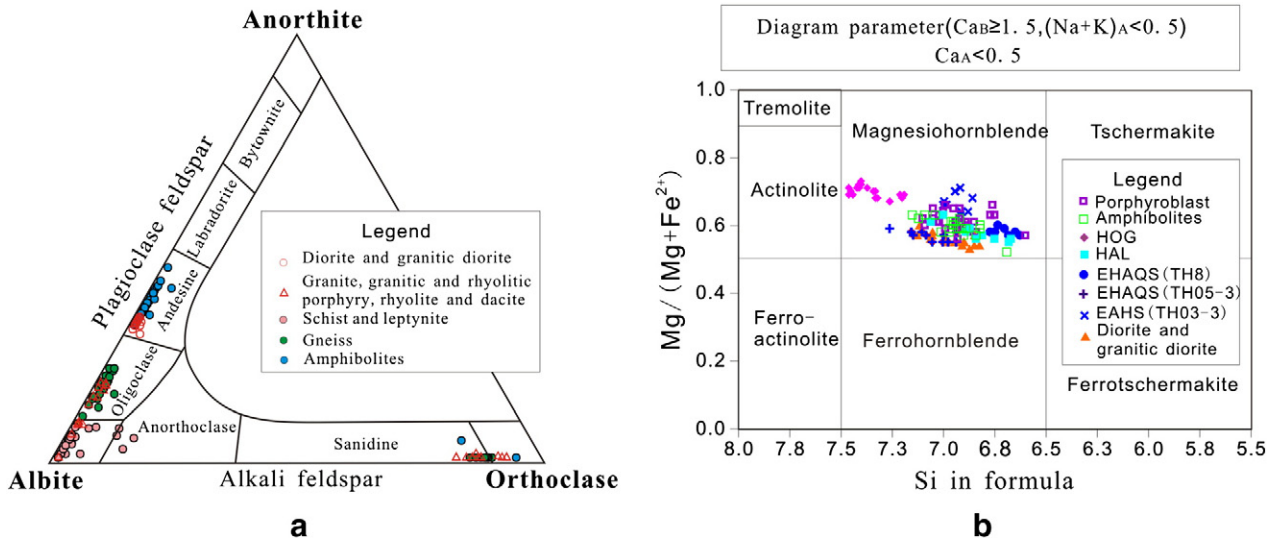

Fig. 9. Composition of feldspar plotted on the Anorthite–Albite–Orthoclase diagram (a) and hornblende plotted in the nomenclature diagram after Leake et al. (1997) (b) for metamorphic and igneous rocks from the Taheir tectonic window. HOG: hornblende oligoclase gneiss, HAL: hornblende albite leptynite, EHAQS: epidote–hornblende–albite–quartz schist, EAHS: epidote–albite–hornblende schist.

andesine from the amphibolite has an anorthite content of 33–46%. Most K-feldspar from the igneous rocks, gneiss and amphibolites are sanidine and orthoclase, with an orthoclase content of >73%.

Amphiboles from metamorphic rocks, diorite and granitic diorite are hornblendes with diagnostic parameters that include Ca_B = 1.73–1.94, $(K+Na)_A$ = 0.15–0.45, $Mg/(Mg+Fe^{2+})$ = 0.52–0.73, and plot in the field of tschermakite in the nomenclature diagram shown in Fig. 9b (Leake et al., 1997). However, hornblendes from different metamorphic and igneous rocks have a variety of compositions. For example, hornblendes from hornblende oligoclase gneiss have high SiO_2 (48.61–51.46 wt.%) and MgO (13.28–14.29 wt.%), and low Al_2O_3 (3.92–5.73 wt.%) and FeO (13.14–15.22 wt.%) contents, while those from an epidote–hornblende–albite–quartz schist in foliated granite have low SiO_2 (44.86–46.08 wt.%) and MgO (10.1–10.81 wt.%) and high Al_2O_3 (8.14–8.81 wt.%) and FeO (18.77–19.68 wt.%) contents (Supplementary Table 1). Hornblendes from the amphibolites contain higher Al_2O_3 (5.73–9.68 wt.%) and FeO (16.19–20.3 wt.%) and lower SiO_2 (44.05–44.82 wt.%) and MgO (9.39–12.39 wt.%) contents than those from gneiss. Hornblendes from the diorite and granitic diorite have low $Mg/(Mg+Fe^{2+})$ values of 0.54–0.61.

5.2.2. Protolith composition

On the assumption that the compositional alterations of these schists, leptynites, gneisses and amphibolites during metamorphism are negligible, the protolithic composition of some representative schists, leptynites, gneisses, amphibolites and micro breccias are estimated according to their mineral assemblages, contents and compositions. The obtained protolithic compositions show that the amphibolites and albite hornblende schists are metamorphosed equivalents of basaltic andesitic tuffs and the hornblende oligoclase gneisses were derived from andesitic and trachytic tuffs (Supplementary Table 1, Fig. 6a). 6 of the 9 studied lava micro breccias are rhyolite, while the other two are trachyte, and the remaining one is trachyandesite. All of these lava micro breccias, medium grade metamorphic rocks and their protolithic tuffs are calc-alkaline (Fig. 6b). This is consistent with the whole rock geochemistry described above.

5.3. Sr and Nd isotope data

The Rb, Sr, Sm and Nd concentrations, $^{143}Nd/^{144}Nd$ and $^{87}Sr/^{86}Sr$ ratios, and T_{DM} ages for igneous rocks in Taheir area are listed in Table 3. The initial $^{143}Nd/^{144}Nd$ and $^{87}Sr/^{86}Sr$ ratios and $\varepsilon_{Nd\ (t)}$ values have been calculated at their corresponding zircon U–Pb concordia age reported below. Depleted mantle model ages (T_{DM}) are reported using the model of DePaolo (1981).

The early Paleozoic igneous rocks, including metamorphic lavas, granitic porphyries, granites and granitic diorite, have low $^{147}Sm/^{144}Nd$ values ranging from 0.1156 to 0.126725, and plot in the field of Andean andesite in the $^{143}Nd/^{144}Nd$ versus $^{143}Sm/^{144}Nd$ plot (Fig. 10a; Goldstein

Table 3
Sm-Nd-Rb-Sr isotope data for igneous rocks from the Taheir area, East Junggar.

Sample	Age (Ma)	Sm (ppm)	Nd (ppm)	$^{147}Sm/^{144}Nd$	$^{143}Nd/^{144}Nd$	$(^{143}Nd/^{144}Nd)i$	$(^{143}Nd/^{144}Nd)_{chur(t)}$	$\varepsilon_{Nd(t)}$	T_{DM} (Ma)	Rb (ppm)	Sr (ppm)	$^{87}Rb/^{86}Sr$	$^{87}Sr/^{86}Sr$	Error (2σ)	$(^{87}Sr/^{86}Sr)i$
TH1	432	1.949	9.826	0.119935	0.512747	0.512407	0.512081	6.36	656	27.28	583.0	0.135388	0.704997	0.000011	0.704164
TH5	446	3.118	11.16	0.143932	0.512818	0.512398	0.512063	6.53	726	25.81	118.8	0.628928	0.707298	0.000012	0.703302
TH6	443	5.330	26.17	0.115600	0.512664	0.512328	0.512067	5.10	756	19.90	232.7	0.247457	0.705937	0.000012	0.704358
TH7	406	4.025	13.27	0.183330	0.512974	0.512486	0.512115	7.25	885	15.20	532.1	0.082670	0.704858	0.000013	0.704380
TH8	432	4.96	24.22	0.1240	0.512671	0.512320	0.512081	4.66	814	20.02	554.6	0.1044	0.705305	0.000009	0.704647
TH9	432	3.210	12.57	0.126725	0.512817	0.512459	0.512081	7.37	583	33.38	778.7	0.124038	0.704957	0.000009	0.704194
ZF5	390	4.701	17.63	0.161240	0.512927	0.512515	0.512136	7.42	648	19.71	494.6	0.115345	0.706054	0.00001	0.705413
ZF8	398	7.580	31.99	0.143239	0.512682	0.512309	0.512125	3.58	1,011	18.41	121.8	0.437416	0.706862	0.00001	0.704370
ZF10-1	455	6.320	32.80	0.116483	0.512689	0.512342	0.512052	5.67	723	17.82	158.6	0.325256	0.706931	0.000011	0.704799
TH02-3	442	4.64	22.52	0.1248	0.512681	0.512319	0.512069	4.90	805	5.516	275.0	0.0580	0.704955	0.000012	0.704591
TH03-3	440	5.78	29.82	0.1172	0.512666	0.512328	0.512071	5.02	765	27.60	142.9	0.5590	0.707522	0.000013	0.704018
TH05-1	416	5.45	18.51	0.1783	0.512983	0.512509	0.512115	7.68	721	19.13	634.5	0.0873	0.704902	0.000012	0.704397
TH05-2	454	5.37	27.84	0.1167	0.512668	0.512321	0.512053	5.23	758	26.91	246.7	0.3157	0.706658	0.000011	0.704611
TH05-3	453	5.48	26.99	0.1230	0.512672	0.512307	0.512054	4.93	804	6.999	307.8	0.0658	0.705258	0.000012	0.704833

Please cite this article as: Xu, X.-W., et al., Tectonic evolution of the East Junggar terrane: Evidence from the Taheir tectonic window, Xinjiang, China, Gondwana Research (2012), http://dx.doi.org/10.1016/j.gr.2012.11.007

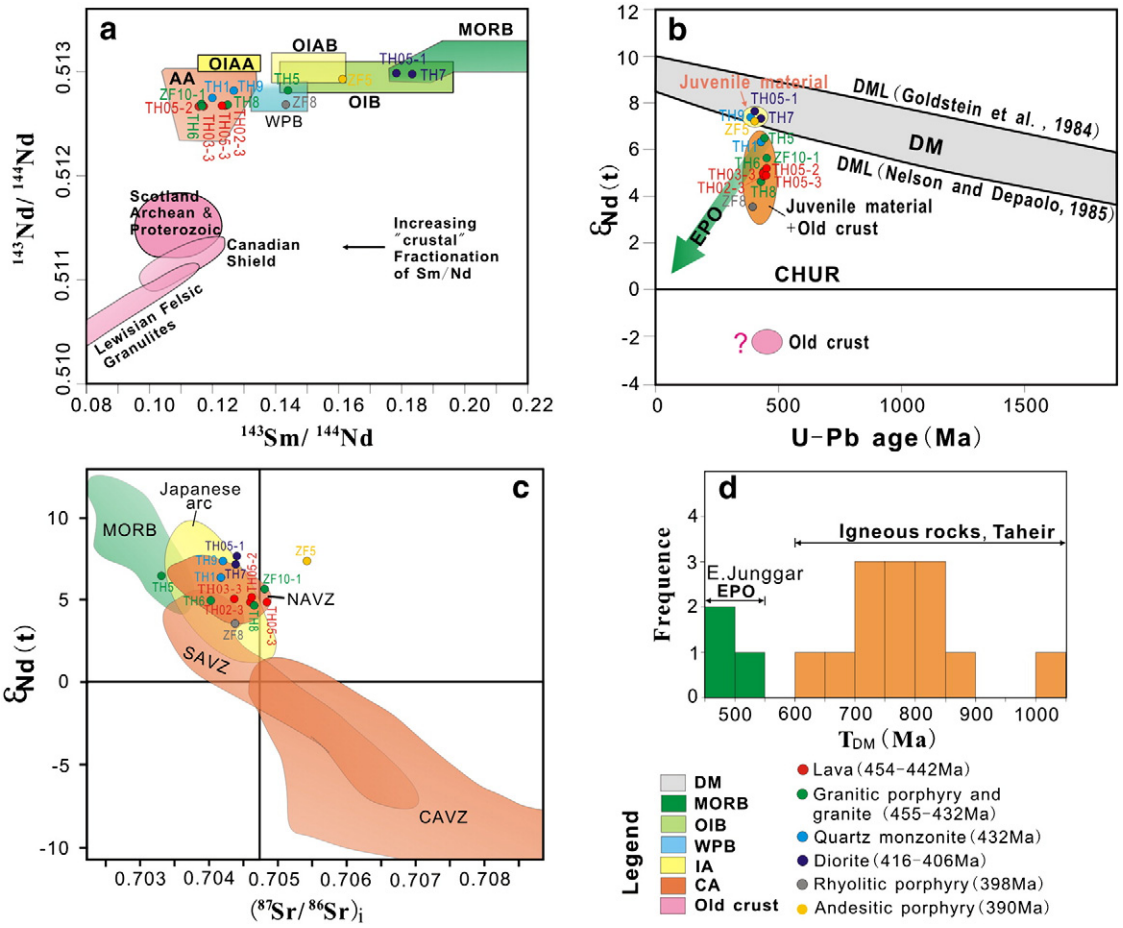

Fig. 10. $^{143}Nd/^{144}Nd$ versus $^{143}Sm/^{144}Nd$ (after Goldstein et al., 1984; Nelson and Depaolo, 1985) (a), Nd isotope (b) and $\varepsilon_{Nd(t)}$ versus $(^{87}Sr/^{86}Sr)_i$ (after Winter, 2001) (d) plots and spectra of the T_{DM} (c) for igneous rocks from the Taheir area. AA: Andean andesite, CAVZ: Central Andean volcanic zone, DM: depleted mantle, DML: depleted mantle line, EPO: early Paleozoic ophiolite in East Junggar, OIAA: oceanic island arc andesite, OIAB: oceanic island arc basalt, MORB: midocean ridge basalts, NAVC: North Andean volcanic zone, OIB: oceanic island basalt, SAVZ: South Andean volcanic zone, WPB: within plate basalts.

et al., 1984), whereas two diorites have high $^{147}Sm/^{144}Nd$ values of 0.1783 and 0.18333.

The $\varepsilon_{Nd\ (t)}$ values and initial $^{87}Sr/^{86}Sr$ ratios of igneous rocks in the Taheir area range from +3.5 to +7.68 and from 0.703302 to 0.705413, respectively. Plots of these rocks in the Nd isotope diagram (Fig. 10b) display four points (diorite, andesitic porphyry and granitic diorite) near the depleted mantle line proposed by Nelson and Depaolo (1985), and the other points extend downwards. Data points in the $\varepsilon_{Nd\ (t)}$ versus $(^{87}Sr/^{86}Sr)_i$ diagram (Fig. 10c) are located mostly in, and a few adjacent to, the North Andean volcanic zone or the Japanese arc fields. These igneous rocks have $T_{DM\ (Nd)}$ ages between 1011 Ma and 583 Ma, which are older than the oldest ophiolite in East Junggar (Fig. 10d).

5.4. Zircon features, U–Pb ages and Lu–Hf isotopes

The CL images of representative zircons selected for U–Pb dating and Hf analyses are shown in Fig. 11. SIMS zircon U–Th–Pb isotopic data are presented in Supplementary Table 2 and illustrated in Fig. 12. LA-ICPMS zircon Hf isotopic data are reported in Supplementary Table 3. The initial $\varepsilon_{Hf\ (t)}$ values and corresponding depleted mantle model ages ($T_{DM\ (Hf)}$) have been calculated at their corresponding zircon $^{206}Pb/^{238}U$ age.

Three metamorphosed lavas, including the rhyolite block (TH05-2), dacite (TH05-3) and trachyandesite (TH02-3), contain zircons that have concentric oscillatory zoning and gray color in CL images and euhedral-to-subhedral and equant-to-stubby forms with average elongation ratios of approximately 1.5 (Figs. 11a, 12b and d). Zircons from sample TH05-2 (rhyolite block) have 108–222 ppm U, 60–229 ppm Th and 10–23 ppm Pb with Th/U ratios in the range of 0.56–1.03, $^{206}Pb/^{238}U$ ages ranging from 448.3 ± 6.5 Ma to 466.6 ± 6.8 Ma with a concordia age of 454.4 ± 1.7 Ma (MSWD = 0.13) (Supplementary Table 2, Fig. 12a), and $^{176}Hf/^{177}Hf$ values from 0.282816 to 0.282915, $\varepsilon_{Hf\ (t)}$ values from +11.3 to +14.6, and $T_{DM2(Hf)}$ ages from 503 Ma to 722 Ma for 14 analyzed crystals (Supplementary Table 3). Zircons from sample TH05-3 (dacite) contain 38–126 ppm U, 19–93 ppm Th and 3–12 ppm Pb with Th/U ratios in the range of 0.52–0.83 and have $^{206}Pb/^{238}U$ ages ranging from 441.2 ± 6.4 Ma to 478.3 ± 8.4 Ma with a concordia age of 453.0 ± 4.4 Ma (MSWD = 0.67) (Supplementary Table 2, Fig. 12b), $^{176}Hf/^{177}Hf$ values from 0.28283 to 0.282894, $\varepsilon_{Hf\ (t)}$ values from +2.4 to +13.9, and $T_{DM2(Hf)}$ ages from 545 Ma to 933 Ma (Supplementary Table 3). Zircons from sample TH02-3 have 30–218 ppm U, 19–271 ppm Th and 3–23 ppm Pb with Th/U ratios in the range of 0.54–1.24, and $^{206}Pb/^{238}U$ ages ranging from 433.2 ± 6.6 Ma to 456.5 ± 7.1 Ma with a concordia age of 442.4 ± 1.9 Ma (MSWD = 0.21) for 12 analyzed single crystals (Supplementary Table 2, Fig. 12c), $^{176}Hf/^{177}Hf$ values from 0.282326 to 0.282938, $\varepsilon_{Hf\ (t)}$ values from −6.4 to +14.9, and $T_{DM2(Hf)}$ ages from 465 Ma to 1829 Ma for 20 analyses (Supplementary Table 3).

Another trachyte block (sample TH03-3) contains euhedral-to-subhedral and stubby zircons with bright rims and gray cores and some anhedral detrital zircons (Fig. 11c). The results of 11 analyses on 11 single zircons revealed that they have U–Pb–Hf isotopic compositions as follows: 32–190 ppm U, 18–220 ppm Th and 3–19 ppm Pb, Th/U ratios from 0.57 to 1.16, $^{206}Pb/^{238}U$ ages range from 429.5 ± 6.4 Ma to 453.2 ± 6.6 Ma with a concordia age of 441.7 ± 2.0 Ma

Please cite this article as: Xu, X.-W., et al., Tectonic evolution of the East Junggar terrane: Evidence from the Taheir tectonic window, Xinjiang, China, Gondwana Research (2012), http://dx.doi.org/10.1016/j.gr.2012.11.007

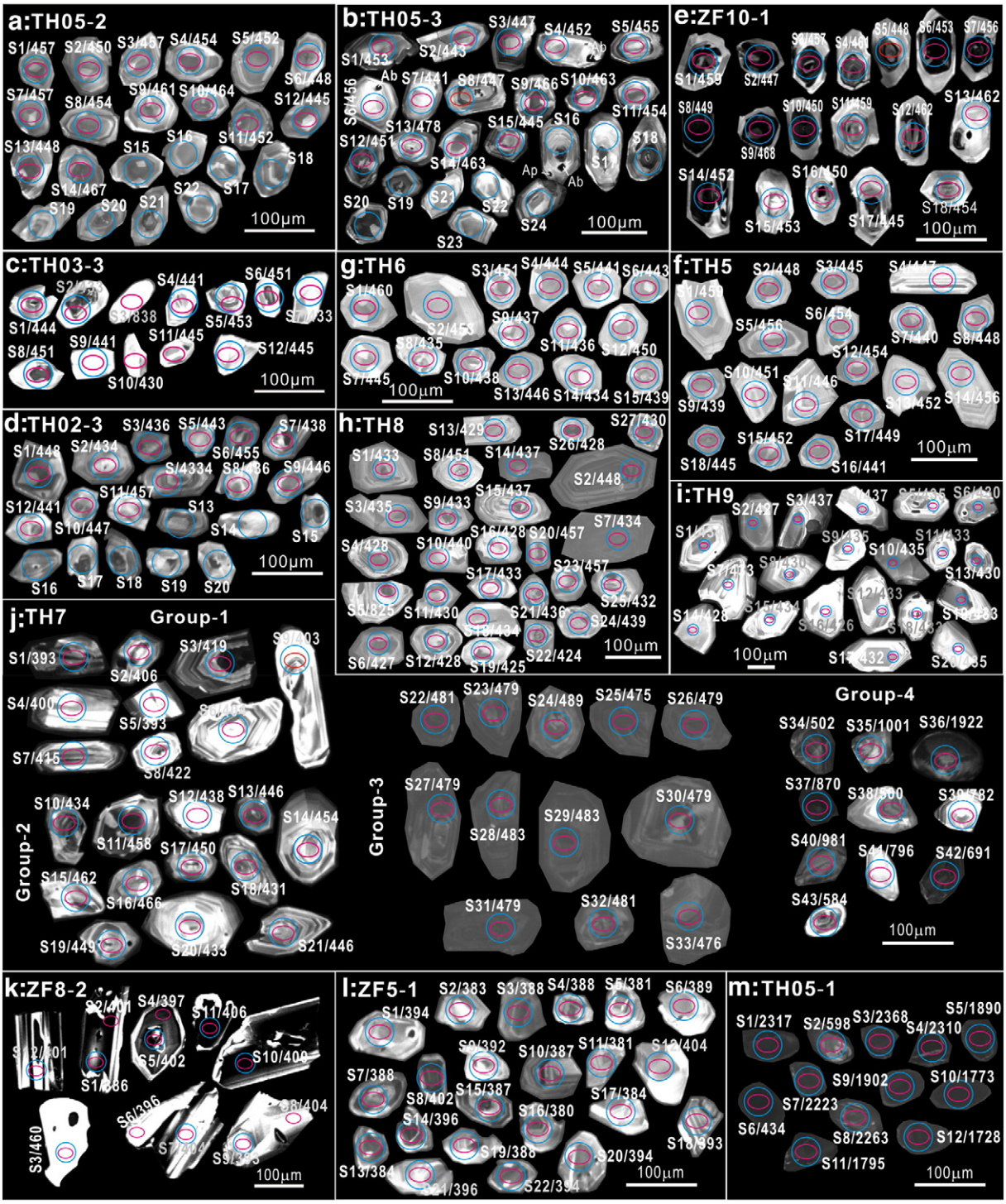

Fig. 11. Cathodoluminescence (CL) images of representative zircon grains selected for SIMS U–Pb dating and LA–ICPMS Hf isotope analysis from igneous rocks from the Taheir area. The red ellipses show the location and size of laser ablating for SIMS U–Pb dating, while the blue circle for LA–ICPMS Hf isotope analysis. The spot number and $^{206}Pb/^{238}U$ age number of zircon was labeled aside the red ellipses and blue circle. Ab: albite, Ap: apatite.

(MSWD = 0.17) (Supplementary Table 2, Fig. 12d), and $^{176}Hf/^{177}Hf$ values from 0.282698 to 0.282900, $\varepsilon_{Hf\,(t)}$ values from +6.3 to +13.2, and $T_{DM2(Hf)}$ ages from 530 Ma to 1008 Ma (Supplementary Table 3). A detrital zircon (S3 in Fig. 11c) contains 107 ppm U, 235 ppm Th and 26 ppm Pb with Th/U ratios of 2.19 and has $^{206}Pb/^{238}U$ age of 837.6 ± 12.0 Ma, a $^{176}Hf/^{177}Hf$ value of 0.282963, and a $\varepsilon_{Hf\,(t)}$ value of +5.5, corresponding to a $T_{DM2(Hf)}$ age of 1382 Ma.

All the weakly deformed granitic porphyries (sample ZF10-1 and TH5) and granite (sample TH6) have zircons that are euhedral to subhedral and equant to stubby with average elongation ratios of approximately 1.6 and concentric oscillatory zoning (Figs. 11e, 12f and g). The 18 analyzed zircon crystals from sample ZF10-1 have gray rims and dark cores in the CL images, and have 31–644 ppm U, 17–1482 ppm Th and 3–84 ppm Pb, Th/U ratios from 0.56 to 2.3, $^{206}Pb/^{238}U$ ages ranging from 444.8 ± 7.1 Ma to 468.1 ± 7.6 Ma with a concordia age of 455.4 ± 1.7 Ma (MSWD = 0.43) (Supplementary Table 2, Fig. 12e), $^{176}Hf/^{177}Hf$ values from 0.282022 to 0.282920, $\varepsilon_{Hf\,(t)}$ values from −16.9 to +14.9, and $T_{DM2(Hf)}$ ages from 495 Ma to

Please cite this article as: Xu, X.-W., et al., Tectonic evolution of the East Junggar terrane: Evidence from the Taheir tectonic window, Xinjiang, China, Gondwana Research (2012), http://dx.doi.org/10.1016/j.gr.2012.11.007

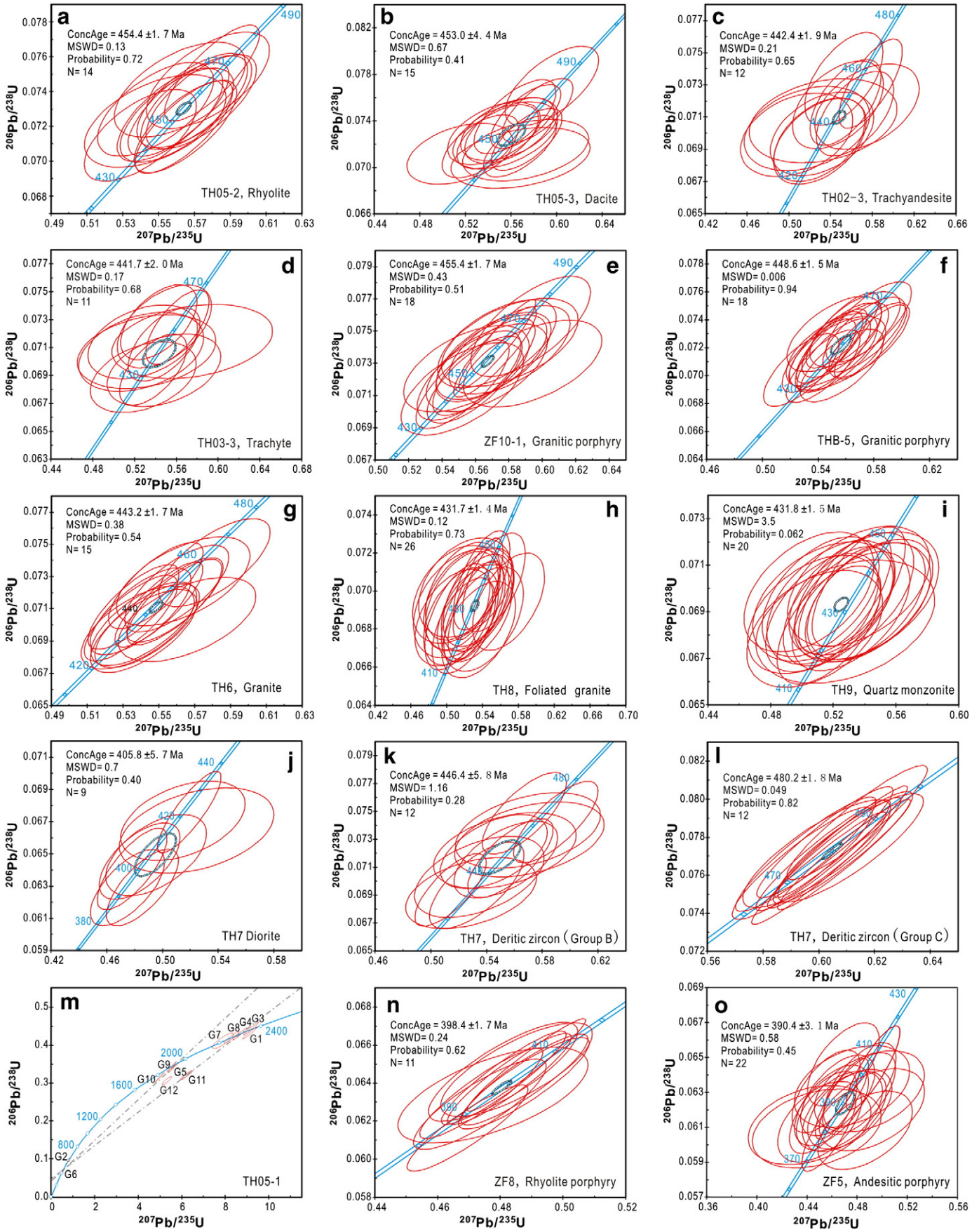

Fig. 12. Zircon SIMS U–Pb concordia age plots of igneous rocks from the Taheir area.

Please cite this article as: Xu, X.-W., et al., Tectonic evolution of the East Junggar terrane: Evidence from the Taheir tectonic window, Xinjiang, China, Gondwana Research (2012), http://dx.doi.org/10.1016/j.gr.2012.11.007

2503 Ma (Supplementary Table 3). Zircons from sample TH5 contain 57–268 ppm U, 28–236 ppm Th and 5–27 ppm Pb with Th/U ratios from 0.31 to 0.88 and have $^{206}Pb/^{238}U$ ages ranging from 438.7 ± 6.4 Ma to 468.1 ± 7.6 Ma with a concordia age of 448.6 ± 1.5 Ma (MSWD = 0.006) (Supplementary Table 2, Fig. 12f), $^{176}Hf/^{177}Hf$ values from 0.282785 to 0.282934, $\varepsilon_{Hf\ (t)}$ values from +9.7 to +15.0, and $T_{DM2(Hf)}$ ages from 472 Ma to 811 Ma for 18 analyzed crystals (Supplementary Table 3). Zircons from sample TH6 have 82–278 ppm U, 28–261 ppm Th and 7–30 ppm Pb with Th/U ratios from 0.44 to 1.33, have $^{206}Pb/^{238}U$ ages ranging from 434 ± 6.3 Ma to 459.5 ± 6.7 Ma with a concordia age of 443.2 ± 1.7 Ma (MSWD = 0.38) (Supplementary Table 2, Fig. 12f), $^{176}Hf/^{177}Hf$ values from 0.282823 to 0.282925, $\varepsilon_{Hf\ (t)}$ values from +10.9 to +14.7, and $T_{DM2(Hf)}$ ages from 492 Ma to 726 Ma for 15 analyzed crystals (Supplementary Table 3).

The intensely deformed granite (sample TH8) contains zircons that are euhedral to subhedral and stubby with average elongation ratios of approximately 1.6 and concentric oscillatory zoning with bright-gray color in CL images (Fig. 11h). Few of them have primary zircon cores. The results of 26 analyses on 26 single zircons revealed that they have the following U–Pb–Hf isotopic compositions: 44–296 ppm U, 22–240 ppm Th and 4–26 ppm Pb, Th/U ratios from 0.37 to 0.96, $^{206}Pb/^{238}U$ ages ranging from 424 ± 6.2 Ma to 457.4 ± 6.6 Ma with a concordia age of the following 431.7 ± 1.4 Ma (MSWD = 0.12) (Supplementary Table 2, Fig. 12h), $^{176}Hf/^{177}Hf$ values from 0.282356 to 0.282974, $\varepsilon_{Hf\ (t)}$ values from −5.6 to +15, and $T_{DM2(Hf)}$ ages from 455 Ma to 1786 Ma (Supplementary Table 3). One primary zircon core (spot 5) contains 537 ppm U, 135 ppm Th and 83 ppm Pb with Th/U ratios of approximately 0.25 and has a $^{206}Pb/^{238}U$ age of 824.8 ± 12.1 Ma, a $^{176}Hf/^{177}Hf$ value of approximately 0.282963, and a $\varepsilon_{Hf\ (t)}$ value of +5.2 with a $T_{DM2(Hf)}$ age of 1390 Ma.

The granitic diorite (sample TH9) has relatively larger zircons that are euhedral to subhedral and equant to stubby forms with length ranging from 127 μm to 258 μm with elongation ratios from 1.0 to 2.2 (Fig. 11i). The 20 analyses on the 20 single zircons show that these zircon have 21–100 ppm U, 10–33 ppm Th and 2–8 ppm Pb with Th/U ratios from 0.3 to 0.65, $^{206}Pb/^{238}U$ ages ranging from 425.8 ± 6.2 Ma to 436.8 ± 6.3 Ma with a concordia age of 431.8 ± 1.5 Ma (MSWD = 3.5) (Supplementary Table 2, Fig. 12i), $^{176}Hf/^{177}Hf$ values from 0.282889 to 0.282943, $\varepsilon_{Hf\ (t)}$ values from +13.3 to +15.2, and $T_{DM2(Hf)}$ ages from 448 Ma to 567 Ma (Supplementary Table 3).

The diorites contain only few zircons. Only about 150 zircon grains were separated from a 100 kg rock sample (sample Th7) from a diorite stock; these zircons can be divided into four groups (Fig. 11j). Group-A zircons are euhedral to subhedral, have concentric oscillatory zoning and stubby forms with average elongation ratios of approximately 2.0 and have 83–553 ppm U, 40–311 ppm Th and 6–46 ppm Pb with Th/U ratios from 0.45 to 1.15, $^{206}Pb/^{238}U$ ages ranging from 393.3 ± 5.3 Ma to 421.7 ± 6.2 Ma with a concordia age of 405.8 ± 5.7 Ma (MSWD = 0.7) (Supplementary Table 2, Fig. 12j), $^{176}Hf/^{177}Hf$ values from 0.282233 to 0.282720, $\varepsilon_{Hf\ (t)}$ values from −11 to +6.3, and $T_{DM2(Hf)}$ ages from 989 Ma to 2089 Ma for 9 analyses (Supplementary Table 3). Group-B zircons are euhedral to subhedral, have concentric oscillatory zoning and equant to stubby forms with average elongation ratios of approximately 1.5 and have 67–278 ppm U, 34–139 ppm Th and 6–23 ppm Pb with Th/U ratios from 0.38 to 0.72, $^{206}Pb/^{238}U$ ages ranging from 431.2 ± 6.3 Ma to 465.5 ± 7.2 Ma with a concordia age of 446.4 ± 5.8 Ma (MSWD = 1.16) (Supplementary Table 2, Fig. 12k), $^{176}Hf/^{177}Hf$ values from 0.282669 to 0.282939, $\varepsilon_{Hf\ (t)}$ values from +5.7 to +15.1, and $T_{DM2(Hf)}$ ages from 465 Ma to 1657 Ma for 12 analyses (Supplementary Table 3). Group-C zircons are unitary and have a dark-gray color and concentric oscillatory zoning in the CL images, have euhedral to subhedral and equant to stubby forms with average elongation ratios of approximately 1.5, and have 483–3068 ppm U, 304–1111 ppm Th and 48–272 ppm Pb with Th/U ratios from 0.3 to 1.35, $^{206}Pb/^{238}U$ ages range from 474.5 ± 7.2 Ma to 488.8 ± 7.3 Ma with a concordia age of 480.2 ± 1.3 Ma (MSWD = 0.049) (Supplementary Table 2, Fig. 12l), $^{176}Hf/^{177}Hf$ values from 0.282091 to 0.282219, $\varepsilon_{Hf\ (t)}$ values from −14.2 to −9.4, and $T_{DM2(Hf)}$ ages from 2048 Ma to 2344 Ma for 12 analyses (Supplementary Table 3). Group-D zircons vary greatly and have $^{206}Pb/^{238}U$ ages ranging from 500.3 ± 7.4 Ma to 1922.2 ± 25.3 Ma (Supplementary Table 2), and $^{176}Hf/^{177}Hf$ values from 0.281405 to 0.282555 with corresponding $\varepsilon_{Hf\ (t)}$ values from −22.3 to +6.7 and $T_{DM2(Hf)}$ ages from 1257 Ma to 3076 Ma (Supplementary Table 3). Evidence that the diorite stock emplaced and cut the foliated granitic porphyry with a concordia age of 432 Ma indicates that the group-A zircons may have crystallized from diorite and that the other three group zircons are detrital. The group-B zircons may be from ambient rocks, and the unitary group-C zircons may be from a deep-situated granitic pluton.

Sample TH05-1 from a diorite dike (Fig. 1d) yielded about 30 zircon grains from a 5 kg rock sample, and the 12 largest of them were analyzed. These 12 zircon grains are dark-gray, have absent of or indiscernible zoning structures and are round to anhedral. They are equant to stubby forms with lengths ranging from 60 μm to 85 μm with average elongation ratios of approximately 1.5 (Fig. 11m). They have 252–1946 ppm U, 50–384 ppm Th and 29–711 ppm Pb with Th/U ratios from 0.03 to 0.68, $^{206}Pb/^{238}U$ ages ranging from 433.5 ± 6.3 Ma to 2368 ± 29.8 Ma and $^{206}Pb/^{207}Pb$ ages from 372.4 ± 21.2 Ma to 2297.4 ± 4.4 Ma (Supplementary Table 2), $^{176}Hf/^{177}Hf$ values from 0.281281 to 0.282663, $\varepsilon_{Hf\ (t)}$ values from −7.7 to +3.5, and $T_{DM2\ (Hf)}$ ages from 1151 Ma to 2993 Ma for the 12 analyses (Supplementary Table 3). Except for grains G11 and G12, the other 10 zircon grains have concordant ages that plot on or close to the crust evolution line (Fig. 12m). Moreover, error ellipse of ten older (>1800 Ma) zircons is oriented towards the location of G6 plot located. These 12 analyzed zircons may be detrital.

The rhyolitic porphyry does not contain many zircons, and only 9 zircon grains were separated from 10 kg of rocks (sample ZF8). These zircons are euhedral to subhedral and stubby and have bright rims and dark-gray cores and some are anhedral, bright detrital zircons (Fig. 11k). The results of 11 analyses on 8 zircons revealed that they have 145–1780 ppm U, 49–1920 ppm Th and 11–160 ppm Pb with Th/U ratios from 0.33 to 1.08, $^{206}Pb/^{238}U$ ages ranging from 385.6 ± 5.6 Ma to 405.8 ± 6 Ma with a concordia age of 398.4 ± 1.7 Ma (MSWD = 0.24) (Supplementary Table 2, Fig. 12n), $^{176}Hf/^{177}Hf$ values from 0.282579 to 0.282690, $\varepsilon_{Hf\ (t)}$ values from +1.9 to +5.0, and $T_{DM2(Hf)}$ ages from 1065 Ma to 1274 Ma (Supplementary Table 3). A detrital zircon (S3 in Fig. 11k) contains 27 ppm U, 13 ppm Th and 2 ppm Pb with Th/U ratios of 0.47 and has a $^{206}Pb/^{238}U$ age of 460.56 ± 4.7 Ma, a $^{176}Hf/^{177}Hf$ value of about 0.282822, and a $\varepsilon_{Hf\ (t)}$ value of about +11.5, corresponding to a $T_{DM2(Hf)}$ age of 703 Ma.

The andesitic porphyry (sample ZF5) contains dark-gray zircons that have concentric oscillatory zoning and lengths ranging from 59 μm to 107 μm with average elongation ratios of approximately 1.5 (Fig. 11l). The results of 22 analyses on 22 single zircons showed that they have 23–406 ppm U, 9–417 ppm Th and 2–36 ppm Pb with Th/U ratios from 0.22 to 1.03, $^{206}Pb/^{238}U$ ages ranging from 380.2 ± 5.6 Ma to 403.7 ± 5.9 Ma with a concordia age of 390.4 ± 3.1 Ma (MSWD = 0.58) (Supplementary Table 2, Fig. 12o), $^{176}Hf/^{177}Hf$ values from 0.282623 to 0.283016, $\varepsilon_{Hf\ (t)}$ values from +2.7 to +15.3, and $T_{DM2(Hf)}$ ages from 406 Ma to 1210 Ma (Supplementary Table 3).

5.5. Hornblende $^{40}Ar/^{39}Ar$ age

The results from argon isotope dating of hornblende crystals from the diorite (sample TH05-1) and amphibolite (sample ZF10-3) from the lower unit of the Taheir tectonic window are shown in Table 4 and Fig. 13.

Please cite this article as: Xu, X.-W., et al., Tectonic evolution of the East Junggar terrane: Evidence from the Taheir tectonic window, Xinjiang, China, Gondwana Research (2012), http://dx.doi.org/10.1016/j.gr.2012.11.007

Table 4
Summary of argon isotopic results of hornblende from diorite (TH05-1) and amphibolite (ZF10-3) from the Taheir tectonic window.

T(°C)	$(^{40}Ar/^{39}Ar)_m$	$(^{36}Ar/^{39}Ar)_m$	$(^{37}Ar/^{39}Ar)_m$	$^{40}Ar\%$	$^{39}Ar_k(10^{-12}$ mol)	$^{39}Ar_k$ (%)	$^{40}Ar/^{39}Ar_k$	Age(Ma)	±1σ
TH05-1,diorite, W=37.3 mg, J=0.002405									
750	648.78	0.293	8.107	59.8	0.12	1.08	566.2	1550.5	±85
850	460.10	0.155	8.086	63.3	0.16	1.44	417.2	1253.6	±67
930	415.45	0.128	8.148	72.2	0.28	2.53	380.3	1171.7	±44
980	396.17	0.218	9.698	66.1	0.19	1.71	334.7	1065.4	±36
1020	308.09	0.202	9.867	62.5	0.15	1.35	250.9	851.8	±30
1060	186.34	0.132	7.818	68.7	0.23	2.07	148.8	551.8	±25
1120	186.97	0.160	8.877	74.4	0.29	2.62	141.5	528.3	±20
1160	123.38	0.084	6.269	79.8	0.34	3.08	99.40	386.6	±15
1200	127.55	0.061	4.944	95.8	0.62	5.62	110.3	420.8	±10
1250	111.45	0.012	4.107	96.8	3.67	33.4	108.8	418.3	±4
1300	111.65	0.015	4.786	96.1	2.08	18.9	107.9	416.4	±6
1350	111.58	0.021	5.871	94.4	1.35	12.4	106.3	410.6	±7
1400	112.59	0.017	4.332	95.5	1.52	13.8	108.2	417.1	±8
ZF10-3,amphibolte, W=29.3 mg, J=0.002423									
750	533.20	0.1333	3.773	62.8	0.21	1.27	495.5	1423.7	±94
850	415.71	0.0952	3.291	69.3	0.32	1.92	388.7	1198.0	±66
930	269.52	0.0455	3.253	75.5	0.47	2.85	283.9	945.3	±52
980	277.41	0.0759	4.307	73.4	0.42	2.52	256.1	871.6	±45
1050	202.43	0.0506	3.574	70.2	0.68	4.10	188.2	678.4	±38
1100	168.71	0.0677	3.630	74.2	0.43	2.61	149.4	557.7	±33
1140	113.82	0.0764	4.802	79.4	0.37	2.24	81.90	528.3	±26
1180	116.12	0.0551	4.012	90.8	0.71	4.30	101.9	398.2	±18
1220	110.62	0.0247	3.815	93.9	1.17	7.09	103.9	405.4	±14
1280	109.66	0.0136	3.425	98.1	3.86	23.4	106.8	415.6	±8
1350	106.69	0.0073	3.434	97.8	5.92	35.9	105.1	416.4	±6
1400	107.91	0.0149	5.195	96.5	1.94	11.8	104.3	410.6	±10

The hornblendes from the diorite (sample TH05-1) yield a $^{40}Ar/^{39}Ar$ plateau age of 416±6 Ma (at increments 8–13; 83.6% of ^{39}Ar released) with a normal isochron age of 414±6 Ma (Fig. 13a and b), and an overprinting age of 387 Ma with a ^{39}Ar content of 3.08% at increment 8. The hornblendes from amphibolite (sample ZF10-3) have $^{40}Ar/^{39}Ar$ ages from 398 to 416 Ma (increments 7–11), which yield a

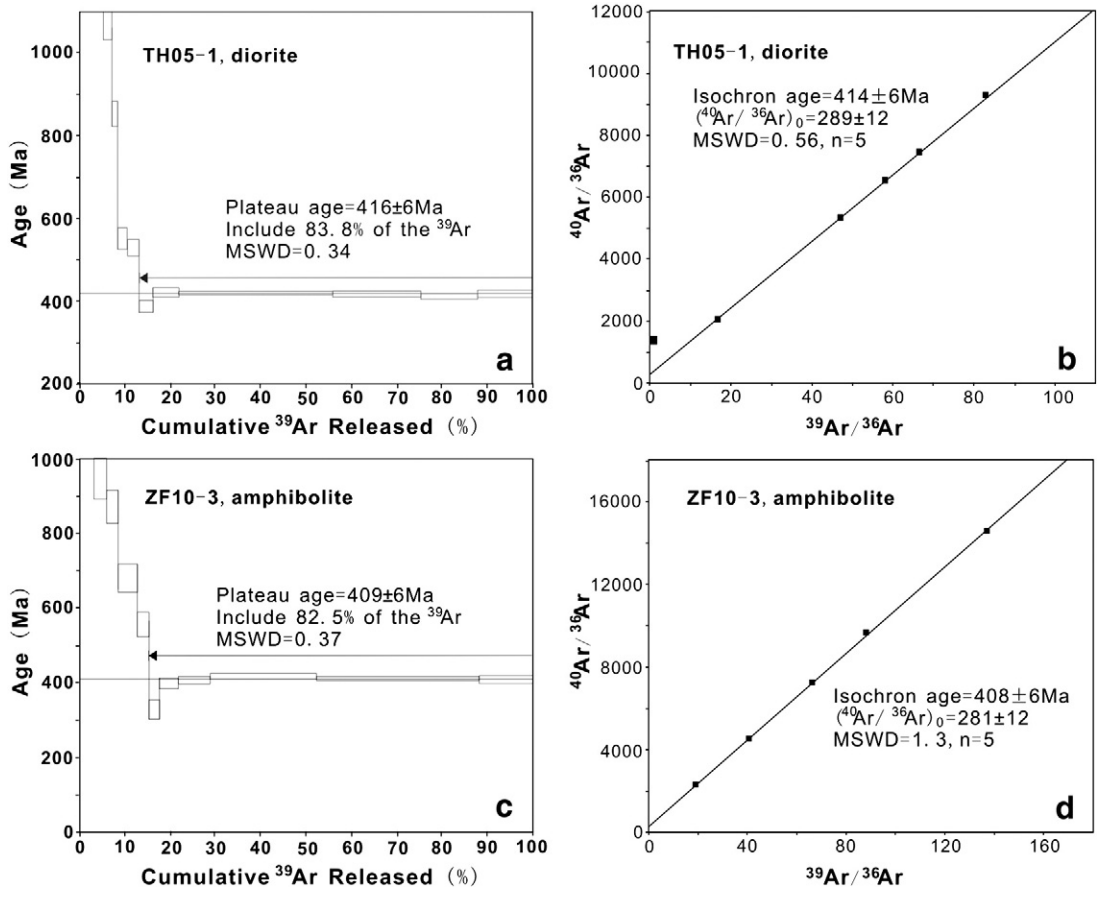

Fig. 13. $^{40}Ar/^{39}Ar$ plateau and isochron ages of hornblende from diorite (a and b) and amphibolite (c and d) from the Taheir tectonic window.

$^{40}Ar/^{39}Ar$ plateau age of 409 ± 6 Ma (82.5% of ^{39}Ar released) with a normal isochron age of 408 ± 8 Ma (Fig. 13c and d).

6. Discussion

6.1. Age spectrum of volcanic, intrusive, metamorphic and deformation events

Zircons from weakly metamorphosed lava and foliated granitic porphyries and granites in the Taheir tectonic window have well developed concentric oscillatory zoning, which is typical of magmatic zircons (Corfu et al., 2003). This indicates that the zircon U–Pb ages reported above should represent the crystallization age of zircons and their host igneous rocks. Lavas from the lower and upper units have ages of 454–453 Ma and 442 Ma, respectively, granitic porphyries were emplaced between 454 Ma and 449 Ma, and granites intruded between 443 Ma and 432 Ma. Therefore, the Taheir tectonic window, composed of metamorphic volcanic rocks, deformed granites and granitic porphyries, and the undeformed granitic diorite, belongs to the early Paleozoic era.

The existence of 480 Ma granitic plutons represented by the Group-C detrital zircons in sample TH7 from a diorite suggests that magmatism in the Taheir area began before 480 Ma. Based on the evidence that the 432 Ma granite (sample TH8) was intensely foliated and underwent low- to medium-grade metamorphism, and the undeformed granitic diorite was intruded into the metamorphic volcanic rocks at 432 Ma, it is suggested that the main deformation and metamorphic event formed the low- to medium-grade metamorphic rocks and granitic mylonite in the Taheir tectonic window is most likely at 432 Ma.

The $^{40}Ar/^{39}Ar$ age of hornblendes and the U–Pb age of zircons from diorites indicate that diorites in the Taheir tectonic window were emplaced from 416 Ma to 406 Ma. The unconformable tectonic event between the Taheir tectonic window and the Devonian volcanic and sedimentary rocks took place between 398 Ma (rhyolitic porphyry, sample ZF8) and 390 Ma (andesitic porphyry, sample ZF5). Volcanism in the Taheir area lasted until the middle Devonian epoch.

The hornblendes from the amphibolite (sample ZF10-3) have $^{40}Ar/^{39}Ar$ ages of 398 Ma, 405 Ma, 410 Ma and 416 Ma with a ^{39}Ar content of approximately 4.3%, 7.09%, 11.8% and 59.1%, respectively. Three of the four $^{40}Ar/^{39}Ar$ ages are very similar to the crystallization ages of the rhyolitic porphyry (sample ZF8, 398 Ma) and a diorite (sample TH7, 406 Ma) and the closure age of another diorite dike (sample TH05-1, 416 Ma). This indicates that these hornblendes have a first closure temperature that is similar to that of the 416 Ma diorite and are overprinted by the 406 Ma diorite and the 398 Ma rhyolitic porphyry.

Additionally, hornblendes both from the analyzed diorite (sample TH05-1) and amphibolite (sample ZF10-3) have $^{40}Ar/^{39}Ar$ ages of 410 Ma with a ^{39}Ar content of 12.4% and 11.8% respectively, strongly implying a intrusive event at this time. It is suggested this intrusion may have resulted in another diorite dike.

6.2. Arc type and evolution of the Taheir tectonic window

All analyzed igneous rocks from the Taheir area show geochemical features of arc-type magmatism, such as low Rb, Nb, Y, Ta and Yb contents, low Ce/Pb values, high K and U contents and Ba/Nb values (Fig. 8a, b, c) (Pearce et al., 1984; Hofmann, 1988; Jahn et al., 1999), and depletion in Nb and enrichment in Pb (Fig. 7b) (Winter, 2001). Moreover, the early Paleozoic igneous rocks have some geochemical features that are different from Devonian igneous rocks in the Taheir area.

6.2.1. The pre-432 Ma Taheir tectonic window arc type

The Ordovician volcanic rocks and granitic porphyries and the Ordovician–Silurian granite show some distinct evidence of Andean-type continental arcs such as the following: 1) geochemical signatures including slight enrichment in LREE, negative Eu anomalies, enrichment in Pb, K and U and depletion in Nb, P and Ti (Winter, 2001), high Th/Yb and Ta/Yb values for a continental arc (Fig. 8d; Pearce, 1983), and high La/Yb values for an Andean-type continental arc (Fig. 8e; Bailey, 1981); 2) calc-alkaline series with high proportions of dacite, rhyolite and andesite, and a large quantity of contemporary granites; and 3) similar Sm–Nd–Rb–Sr isotopic compositions to Andean arc volcanic rocks (Fig. 10a and c). This evidence indicates that the early Paleozoic volcanic rocks, granitic porphyries and granites most likely formed at a continental margin setting. This conclusion is supported by the nature of the basement and other properties of the Taheir crust.

6.2.2. The nature of Taheir crust basement

The basement nature of the Taheir crust can be evaluated from Nd and Hf isotopic signatures. The fact that all the analyzed igneous rocks from the Taheir area have older $T_{DM\ (Nd)}$ ages (583–1011 Ma) than formation ages and the oldest ophiolite in East Junggar (Fig. 10d) indicate that these igneous rocks are mixtures of the juvenile material and old crust (Fig. 10b; Nelson and Depaolo, 1985) and that the older crust is not likely the oldest oceanic crust in East Junggar. Similarly, zircons from these igneous rocks have $\varepsilon_{Hf\ (t)}$ values from +15.9 to −22.3 with $T_{DM2\ (Hf)}$ ages between 405 Ma and 3076 Ma (Supplementary Table 3). It further suggests that these igneous rocks might have been derived from distinct sources related to mixtures of the juvenile material and old crust (Fig. 14) and that a large quantity of old crustal material had been incorporated into these igneous rocks. Evidence from the Paleozoic magmatic zircons in the εHf (t) versus U–Pb age diagram that are present in a rectangle that extend from the depleted mantle line and downward to the 2.5 Ga crust line (Fig. 14) indicate that the old crust may be >2.5 Ga.

The old crustal component of these igneous rocks in the Taheir tectonic window may be directly derived from the old basement formation or the younger sediments with old material (Davidson et al., 2005) or indirectly imparted on the source by the simple subduction of sediment (Tera et al., 1986; Othman et al., 1989; Plank and Langmuir, 1993). If sediments are carried down on the subducted plate, then there must be a similar sedimentary column within the upper plate (Davidson et al., 2005). This means that the Taheir crust should contain old basement formation or sediments with old material. The occurrence of detrital old zircons with straight crystal forms (Fig. 11j and m) indicates that these old zircons should have not suffered long distance transportation and erosion by rive or magma flow and may be from adjacent old formations or rock

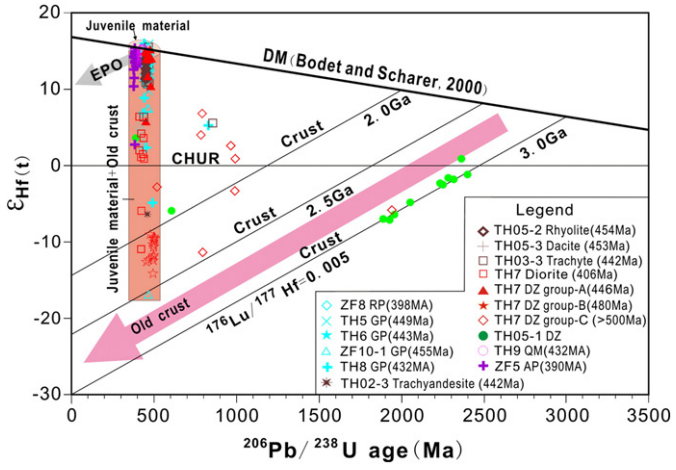

Fig. 14. Diagram of $\varepsilon_{Hf\ (t)}$ versus U–Pb age for zircons from igneous rocks from the Taheir area. Depleted mantle (DM) growth curve from Bodet and Scharer (2000). CHUR, chondritic uniform reservoir. AP: andesitic porphyry, DZ: detrital zircon, EPO: early Paleozoic ophiolite in East Junggar, GP: granitic porphyry, QM: quartz monzonite, RP: rhyolitic porphyry.

Please cite this article as: Xu, X.-W., et al., Tectonic evolution of the East Junggar terrane: Evidence from the Taheir tectonic window, Xinjiang, China, Gondwana Research (2012), http://dx.doi.org/10.1016/j.gr.2012.11.007

fragments. This suggests that the basement of the Taheir crust contains old basement formation or sediments with old rock fragments and that the Taheir tectonic window should be or have been the margins of an ancient continent. Additionally, the nine older (>1800 Ma) zircons of sample TH05-1 plotting along the 3.0 Ga crustal line (Fig. 14) show that the ancient continent may have contained 3.0 Ga crust.

6.2.3. The density of the Taheir crust

The occurrences of glomerocrysts with accumulated structures (Figs. 2e and 5a) in rhyolite and rhyolitic porphyries in the Taheir tectonic window imply that these phenocryst populations and associated granite breccia were formed in intermediate magma chambers, and the granitic magma had undergone differentiation (Xu et al., 2009). This suggests that the Taheir crust may have a low density that retarded ascent and caused these granitic magmas to stagnate and form magma chambers and granitic plutons.

6.2.4. The post-432 Ma Taheir tectonic window arc type

The Devonian diorites and andesitic porphyry have some oceanic island arc geochemical characteristics, such as belonging to tholeiite series (Fig. 6a), having a flat REE pattern (Fig. 7a), enrichment in Pb, K, U and Sr and depletion in Nb, Pr and Zr (Fig. 7b; Macdonald et al., 2000), and $\varepsilon_{Hf\ (t)}$ values similar to contemporary depleted mantle (Fig. 10b; Jakeš and White, 1971; Winter, 2001). On the other hand, these rocks have some characteristics of continental crust, such as their $T_{DM\ (Nd)}$ and $T_{DM2\ (Hf)}$ ages older than their formation ages. Moreover, the 398 Ma rhyolitic porphyries have some geochemical signatures that are similar to the pre-432 Ma igneous rocks, such as being of the calc-alkaline series, the slight enrichment in LREE, the negative Eu anomalies, the enrichment in Pb, K and U and the depletion in Nb, P and Ti, and the high Th/Yb and Ta/Yb values, but moderate La/Yb values and plotting in the field of continental island arc (Fig. 8e). The characteristics indicate that the Taheir late Silurian–Devonian arc may be a continental island arc (Bailey, 1981), similar to the Japanese island arc (Taira, 2001). This is consistent with the occurrence of continental island arc-type Silurian graywackes in the Yemaquan area and Carboniferous sedimentary rocks in the East Junggar Basin (Long et al., 2012; Yang et al., 2012). The 432 Ma granitic diorite and dioritic porphyry have geochemical features that are transitional between the pre-432 Ma igneous rocks and the Devonian diorites and andesitic porphyry, such as being calc-alkaline, having a slight enrichment in LREE, having a slight enrichment in Pb, K, U and Sr and depletion in Nb, Th, Pr, P and Ti, and having $\varepsilon_{Hf\ (t)}$ and $\varepsilon_{Nd\ (t)}$ values close to the depleted mantle line. Moreover, the 432 Ma granitic diorite and dioritic porphyry and 398 Ma rhyolitic porphyries have similar La/Yb values and plot in the same field of continental island arc (Fig. 8e). This suggests that the transformation from the Andean-type continental arc to continental island arc for the Taheir arc may have occurred at 432 Ma. This transformation is possibly related to intra-arc rifting and spreading of back arc oceanic basin (Wilson, 1966).

6.3. The tectonic evolution of the Taheir tectonic window

6.3.1. Magma intrusion and tectonic movements

Generally, granite plutons are commonly emplaced in the middle crust at a depth 8–10 km (e.g., Sides, 1980; Guillot et al., 1995; Jowhar, 2001; Tomiya et al., 2010) and porphyries at a depth of between 1 and 6 km, with an average depth of 1.8 km and a modal depth of 2.8 km (Seedorff et al., 2005; Kesler and Wilkinson, 2008). Therefore, the Ordovician volcanic rocks in the Taheir tectonic window were transferred down to the middle crust between 443 Ma and 432 Ma, and subsequently exhumed before 390 Ma. The deformation structures of these Ordovician volcanic rocks indicate that the subsidence and first-stage shear deformation were most likely related to underthrusting, whereas the exhumation was possibly associated with the second-stage horizontal stretching deformation induced by uplifting and rifting.

6.3.2. The tectonic evolution of the Taheir tectonic window and Yemaquan arc

In summary, the Taheir tectonic window consists of Ordovician volcanic rocks formed at continental margins. The lower unit underwent a series of tectonic processes, including 1) progressive burial associated with the intrusion of a 454–449 Ma granitic porphyries at shallow levels; 2) underthrusting and subsidence to a depth in the middle crust, with an intrusion of 443–432 Ma granites along the way, resulting in metamorphism for the albite–hornblende schists and amphibolites; 3) departing from their continental land and formation of continental island arc at 432 Ma; 4) uplifting and exhumation, associated with the intrusion of a 416–406 Ma diorite with geochemical signatures of a continental island arc environment; 5) erosion and retrograde metamorphism; and 6) exhumation between 398 Ma and 390 Ma.

Therefore, the Yemaquan magmatic arc, as the host of the Taheir tectonic window, formed before 480 Ma and evolved from an Andean-type continental arc to a continental island arc after intra-arc rifting at 432 Ma. Additionally, the occurrence of tin deposits in the Kelameili area at the southern side of the Yemaquan arc further indicates that the Yemaquan arc is most likely an Andean-type continental arc and that the locations of these tin deposits represent a landward side and back-arc environment (Kearey et al., 2009) because the tin deposits are specific to Andean-type subduction and tin is absent in oceanic island arcs (Kearey et al., 2009).

Most recently, Yang et al. (2011) reported geochemical data on the Huangyangshan granitoid pluton in the Kelameili area and suggested that these rocks were related to partial melting of an enriched subcontinental lithospheric mantle of the Kelamaili island arc. However, their granitoid rocks have pronounced negative Eu anomaly, and are enrichment in Zr and depleted in Nb, Sr, P and Ti (Table 3 and Fig. 5 of Yang et al., 2011). This is a typical signature of continental arc rather than oceanic island arc, because igneous rocks formed at oceanic island arc are usually enrichment in Sr, Th and P, and depleted in Zr (Bailey, 1981; Ellam and Hawkesworth, 1988; Winter, 2001). Occurrence of the Shareshike Tin deposit associated with the Huangyangshan granitoid pluton indicates that the Kelamaili island arc is not oceanic island arc (Kearey et al., 2009). Moreover, these post-collision granitoid rocks plot in the field of continent–continent collision both in the Nb–Y–Ce and Rb/Nb versus Y/Nb diagram (Fig. 8c and d of Yang et al., 2011), implying that they were formed at continent–continent collision setting. Therefore, evidence from the Huangyangshan granitoid pluton in the Kelameili area also indicates that the Yemaquan arc is a continental arc.

6.4. The tectonic evolution of East Junggar

Tectonic regime of East Junggar is redefined by the regular arrangement of the Erqis Devonian–Carboniferous ophiolite belt; the Sawuer Devonian–Carboniferous oceanic island arc; the Armantai Cambrian–Ordovician ophiolite belt; the Yemaquan Ordovician Andean-type continental arc that became a continental island arc after the Silurian NW-trending intra-arc rifting in the Taheir area at the southern side, the landward side and the backarc environment; and the Kelameili Devonian–Carboniferous ophiolite belt from north to south. According to modern plate tectonics theory (Wilson, 1966), this regime requires that the Junggar ocean represented by the Kelameili ophiolite belt is a type of back-arc basin and that the Junggar block is an ancient continent because intra-arc rifts, as a part of the rifting systems of back-arc basins, are located adjacent to a back-arc basin (Yamaji, 1990) and both the back-arc basin and potential continent should occur at the back side of the continental island arc and away from oceanic crust or oceanic island arc (Wilson, 1966). The arrangement that the Devonian–Carboniferous

Please cite this article as: Xu, X.-W., et al., Tectonic evolution of the East Junggar terrane: Evidence from the Taheir tectonic window, Xinjiang, China, Gondwana Research (2012), http://dx.doi.org/10.1016/j.gr.2012.11.007

Sawuer oceanic island arc occurs on the north side of the Ordovician Yemaquan Andean-type continental arc calls for a southward subduction of the Paleo-Asian oceanic lithosphere, which was presented at the adjacent northern West Junggar Region (Shen et al., 2012).

On the basis of the newly obtained evidence, the tectonic regimes of East Junggar and their potential tectonic setting, we contest a tectonic evolution model for East Junggar in the central part of the Central Asian Orogenic Belt as following (Fig. 15):

1) The Yemaquan Ordovician Andean-type continental arc was formed by the southward subduction of early Paleozoic Paleo-Asian ocean lithosphere beneath the Junggar continent. The Armantai Cambrian–Ordovician ophiolites are relict fragments of the subducted oceanic crust.
2) This subduction began before 480 Ma. The lower unit of the Taheir tectonic window experienced burial metamorphism between 454 Ma and 449 Ma and subsidence to a depth in the middle crust during the period from 443 Ma to 432 Ma. This rapid subsidence is related to regional compression and crust thrusting.
3) The period of approximately 432 Ma marks an important tectonic shifting point. At this time, intra-arc rifts developed at the back side as a result of mantle upwelling that may have been related to the rollback of the subducted oceanic lithosphere, resulting in rift tectonics associated with extension and the formation of amphibolites in the lower unit and rapid exhumation induced by detachment faults in the Taheir area. Some detachment faults cut through the lower crust and propagated into the upper mantle lithosphere of the Junggar continent.
4) When some of these faults cut the upper mantle lithosphere of the Junggar block, new intensive upwelling of the asthenosphere occurred at the edges of these faults and propagated upwards along these faults during the period between 432 Ma and 416 Ma, causing massive normal faulting and rifting and back-arc basin and crustal thinning along the line formed by the Kelameili ophiolite belt. During this period, the granodiorites with a geochemical signature of continental island arcs intruded into the lower unit of the Taheir tectonic window.
5) Continuous rifting caused the lithosphere to break off, resulting in the detachment of the Yemaquan arc from the Junggar continent and the formation of Junggar ocean. These events may have been complete by 416 Ma. Then, the Yemaquan arc behaved as a continental island arc, and the contemporary 416–406 Ma diorites in the Taheir tectonic window have geochemical signature of continental island arc. During this period, many intermediate-acid stock and porphyries associated with porphyry Cu–Mo deposits in the Qiongheba area at the eastern part of Yemaquan arc formed (Dong et al., 2009; Qu et al., 2009; Du et al., 2010).
6) The chronology of the copper-bearing porphyries in Halasu area (Zhang et al., 2004; Zhang et al., 2006; Xiang et al., 2009) indicate that the intra-ocean subduction and the formation of the Sawuer

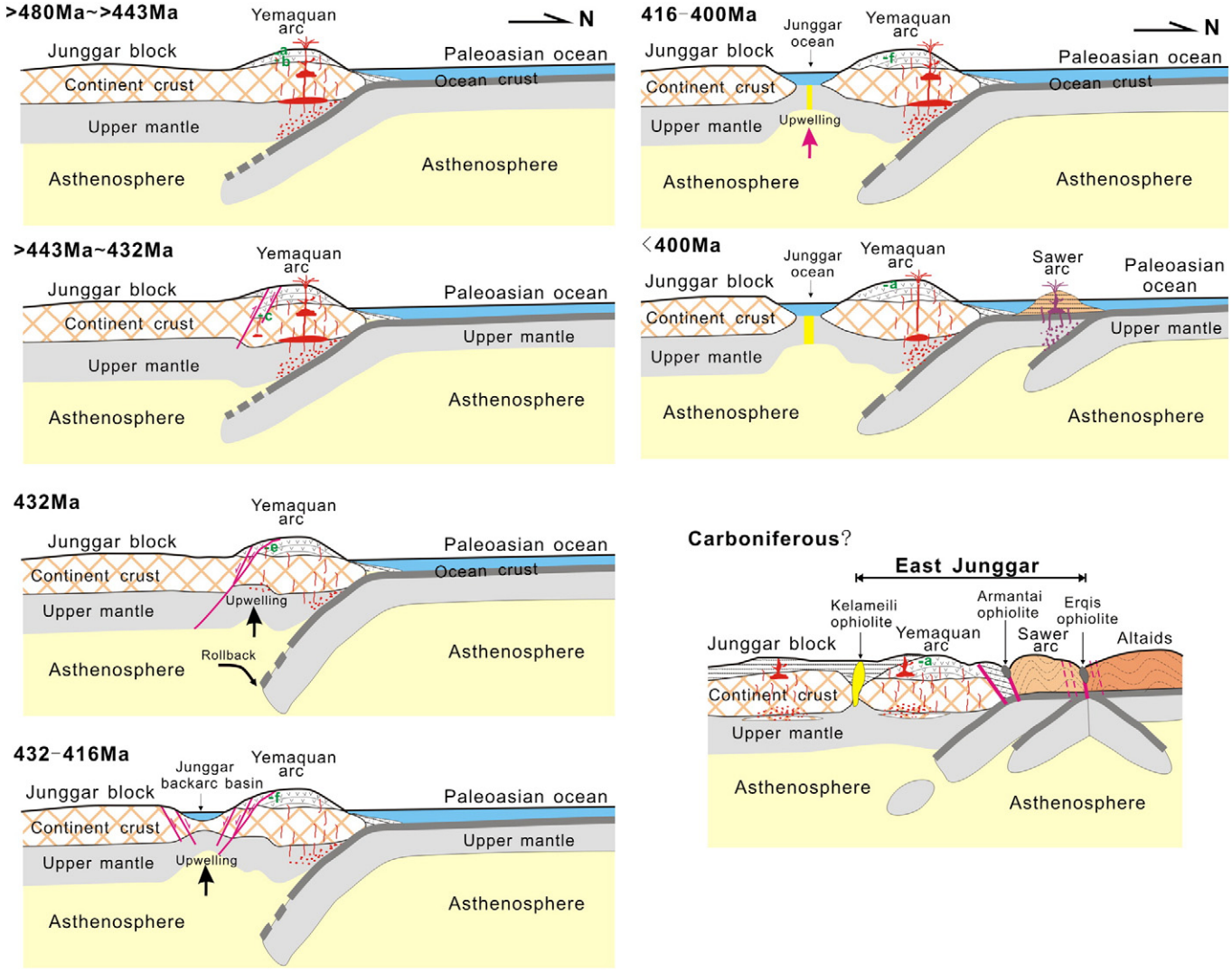

Fig. 15. Tectonic evolution model for the East Junggar. The green dot with label a, b, c, e and f shows the location of the lower unit of the Taheir tectonic window.

Please cite this article as: Xu, X.-W., et al., Tectonic evolution of the East Junggar terrane: Evidence from the Taheir tectonic window, Xinjiang, China, Gondwana Research (2012), http://dx.doi.org/10.1016/j.gr.2012.11.007

arc may have begun at approximately 400 Ma. Namely, at this time, the subduction zone of the Paleoasian oceanic plate retracted from the Armantai area northward to the Erqis area.

7) The fact that the Kelameili ophiolite belt is cut by the Hongliuxia EW-trending ductile shear zone that formed at approximately 344 Ma (Wu et al., 2012) indicates that the collision between the Junggar block, the Yemaquan arc, the Sawuer oceanic island arc and the Altaids may have occurred during the early Carboniferous period before 344 Ma. After 320 Ma, the East Junggar is transited to be post collisional extensional setting, and some related alkaline granites emplaced and volcanic rocks erupted (Su et al., 2008, 2012; Gan et al., 2010; Liu et al., 2012). Then, the present tectonic regime of East Junggar formed. The Kelameili ophiolites are relict fragments of the Junggar back arc oceanic crusts.

This scenario is displayed in the western Pacific region during the Cenozoic era (Taira, 2001). However, additional details of the tectonic processes of formation of the Junggar back arc ocean and the collision events during the early Carboniferous period remain unclear. The Carboniferous volcanic rocks located over the Junggar block may have been formed at the post-collision stage and be related to continental rifting tectonics (Gu et al., 2000).

6.5. Basement nature of the Junggar terrane

The occurrence of Andean-type continental arc in the Taheir area indicates that there should have been a continent in the Junggar terrane in the early Paleozoic. The suggestion that the Paleozoic igneous rocks in the Taheir area are derived from a mixture of the juvenile material and ≥2.5 Ga crust (Fig. 14) indicates that the Taheir tectonic window and its host Junggar terrane have a ≥2.5 Ga basement crust. The nine older (>1800 Ma) zircons from sample TH05-1 plotting along the 3.0 Ga crustal line (Fig. 14) show that the Junggar continent may have contained 3.0 Ga crust. These conclusions are consistent with the documented geological and geophysical features of the Junggar terrane, including (1) the wide angle seismic reflection and magnetotelluric sounding data shows that thickness of crystalline crust of the Junggar basin is about 43–48 km (Zhao et al., 2003), which is greater than that of the modern oceanic crust and oceanic island arc (Mooney et al., 1998; Dimalanta et al., 2002); and (2) the Devonian sandstones in the northeastern Junggar block contain a large number of Pre-Cambrian detrital zircons ranging from 550 Ma up to 3037 Ma (Lin et al., 2007), three of which (grain 9.1, 70.1 and 71.1) are metamorphic zircons with Th/U values ranging from 0.12 to 0.27 and have an concordia age of 953±9.1 Ma (MSWD=4.3).

Recently, Zheng et al. (2007) reported elemental and Sr–Nd–Pb isotopic geochemistry of Late Paleozoic volcanic rocks beneath the Junggar basin and suggested that the basaltic rocks represent trapped late Paleozoic oceanic and the silicic rocks are products of melting of oceanic crust. However, their data do not support their interpretations. For example, six of the seven analyzed basalts are depleted in Nb compared to K, Rb and U, and the La/Nb values of three basalts (sample k178, k204 and k211) are equal or greater than 1.4 (Table 2 of Zheng et al., 2007). This indicates that these basalts are not mid-ocean ridge basalts (MORB) or ocean island basalts (OIB) (Mahoney et al., 1993; Condie, 1999). In contrast, the Nb/U values of the seven basalts are less than 20, showing distinct signature of continental crust (Hofmann et al., 1986). On the other hand, these volcanic rocks do not have geochemical features of adakitic rocks, which are derived from partial melting of oceanic crust (Defant and Drummond, 1990). Moreover, all the Late Paleozoic volcanic rocks plot in the field close to the lower crust and away from MORB and OIB in the $(^{206}Pb/^{204}Pb)_{initial}$ versus $(^{207}Pb/^{204}Pb)_{initial}$ and $(^{208}Pb/^{204}Pb)_{initial}$ diagram (Fig. 8c and d of Zheng et al., 2007). Therefore, the Late Paleozoic volcanic rocks beneath the Junggar basin are most likely derived from continental crust rather than oceanic crust.

More recently, Xiao et al. (2012) reported zircon Hf isotope and whole rock geochemistry of Late Paleozoic magmatic rocks in the Baijiangou and Zhangpenggou area in the northeastern Junggar block and considered the East Junggar terrane as oceanic island arc. However, these magmatic rocks have pronounced negative Eu anomaly, and are enriched in Pb, Rb and U and depleted in Nb, Sr, Th and Ti (Fig. 8 of Xiao et al., 2012), implying that they are not oceanic island arc (Ellam and Hawkesworth, 1988). Moreover, these magmatic rocks plot in the field of continental arc in the Th/Yb versus Nb/Yb diagram (Fig. 9a in the reference of Xiao et al., 2012).

In summary, the Junggar terrane contains Precambrian continent. It is suggested that the accretionary orogeny in the Central Asian Orogenic Belt is more complex than in the previous models proposed by Sengör et al. (1993) and Sengör and Natal'in (1996) and that there may have been some ancient continental fragments, such as Junggar block (Zhao et al., 2003; Charvet et al., 2007), Yili block (Long et al., 2011), central Tienshan (Hu et al., 2006) and southern Kazakhstan micro-continental fragments (Abdulin et al., 1995; Kröner et al., 2007). These continental fragments make the history of accretionary orogenesis more intriguing.

7. Conclusion

The Taheir tectonic window consists of metamorphosed and deformed Ordovician volcanic rocks and granitic porphyries and Ordovician–Silurian granites as well as undeformed Silurian– Devonian granitic diorite, diorites and rhyolitic porphyries.

Ordovician volcanic rocks and granitic porphyries, and Ordovician–Silurian granites in the Taheir tectonic window exhibit some distinct evidence of Andean-type arc continental arcs, including low Rb, Y, Ta and Yb content, low Ce/Pb values, high La/Yb, Ba/Nb, Th/Yb and Ta/Yb values, enrichment in Pb, K and U and depletion in Nb, P and Ti, slight enrichment in LREE, negative Eu anomalies, high proportions of dacite, rhyolite and andesite of the calc-alkaline series, the presence of a large quantity of contemporary granites, similar Sm–Nd–Rb–Sr isotopic composition to Andean volcanic rocks, older $T_{DM\ (Nd)}$ ages (583–1011 Ma) than formation ages, $\varepsilon_{Hf(t)}$ values from +14.9 to −16.9 with $T_{DM2\ (Hf)}$ ages between 465 Ma and 2503 Ma, mixtures of the juvenile material and ≥2.5 Ga crust, intensive crystallization differentiation. These rocks are formed at continental margins.

These Ordovician volcanic rocks underwent a series of tectonic events, including burial metamorphism associated with the intrusion of 454–449 Ma granitic porphyries, underthrusting and subsidence to a depth in the middle crust associated with the intrusion of 443–432 Ma granites and the formation albite–hornblende schists, hornblende–albite–quartz leptynites and amphibolites, departure from continental land and formation of continental island arc around 432 Ma, the exhumation associated with the intrusion of 416–406 Ma diorites with geochemical signatures of a continental island arc, and the erosion and return to the surface between 398 Ma and 390 Ma.

The Taheir tectonic window arc and its host Yemaquan magmatic arc changed from Andean-type continental arc to continental island arc after intra-arc rifting since 432 Ma. The tectonic regime of East Junggar and the adjacent area is redefined by the regular arrangement of the Erqis Devonian–Carboniferous ophiolite belt, the Sawuer Devonian–Carboniferous oceanic island arc, the Armantai Cambrian–Ordovician ophiolite belt, the Yemaquan Ordovician Andean-type continental arc that became a continental island arc after Silurian NW-trending intra-arc rifting at the southern, landward side and in the backarc environment, and the Kelameili Devonian–Carboniferous ophiolite belt from north to south. This regime requires a back-arc basin for the Junggar ocean that is represented by the Kelameili ophiolites and an ancient continent for the Junggar block.

Please cite this article as: Xu, X.-W., et al., Tectonic evolution of the East Junggar terrane: Evidence from the Taheir tectonic window, Xinjiang, China, Gondwana Research (2012), http://dx.doi.org/10.1016/j.gr.2012.11.007

Acknowledgements

This research was supported by the CAS Knowledge Innovation Project (Grant Numbers kzcx-ew-ly03 and kzcx2-yw-107), the National Natural Science Foundation of China (Grant Number 41072060), and the National 305 project (Grant Numbers 2011BAB06B03-3 and 2006BAB07B01-03). We are indebted to X.D. Jin for the arrangement of the trace element analysis, Q. L. Li and Y. Liu for the help in conducting the Cameca IMS-1280 ion microprobe, C.F. Li for the Nd isotope experiment, and Y.G. Ma and X. Yan for assistance with EMP and SEM analyses. We thank K.Z. Qin, W.J. Xiao, J.H. Guo, L.D. Ren, and G.Q. He and S. Sun for valuable discussions. This paper was significantly improved by the thorough and incisive review of three anonymous reviewers.

Appendix A. Supplementary data

Supplementary data to this article can be found online at http://dx.doi.org/10.1016/j.gr.2012.11.007.

References

Abdulin, A.A., Avdeev, A.V., Seitov, N.S., 1995. On the study of microcontinents and ophiolite zones in Kazakhstan. Occasional Publications, ESRI, University of South Carolina, USA, New Series No. 12B, pp. 97–112.
Allen, M.B., Vincent, S.J., 1997. Fault reactivation in the Junggar region, northwest China: the role of basement structures during Mesozoic–Cenozoic compression. Journal of the Geological Society of London 154, 151–155.
Bailey, J.C., 1981. Geochemical criteria for a refined tectonic discrimination of orogenic andesites. Chemical Geology 32, 139–154.
Bazhenov, M.L., Levashova, N.M., Degtyarev, K.E., Van der Voo, R., Abrajevitch, A.V., McCausland, P.J.A., 2012. Unraveling the early–middle Paleozoic paleogeography of Kazakhstan on the basis of Ordovician and Devonian paleomagnetic results. Gondwana Research 22, 974–991.
Biske, Yu.S., Seltmann, R., 2010. Paleozoic Tian-Shan as a transitional region between the Rheic and Urals-Turkestan oceans. Gondwana Research 17, 602–613.
Bodet, F., Scharer, U., 2000. Evolution of the SE-Asian continent from U–Pb and Hf isotopes in single grains of zircon and baddeleyite from large rivers. Geochimica et Cosmochimica Acta 64, 2067–2091.
Boynton, W.V., 1984. Geochemistry of the rare earth elements. Meteorite studies. In: Henderson (Ed.), Rare Earth Element Geochemistry. Elsevier, pp. 63–114.
Bu, G., Li, H., Li, W., Yu, H., Jin, H., 2005. Geochemical characteristics and tectonic settings for basalts in Takezhale ophiolite in East Junggar, Xinjiang. Geotectonica et Metallogenia 29, 252–261 (in Chinese with English abstract).
Buslov, M.M., Fujiwara, Y., Iwata, K., Semakov, N.N., 2004. Late Paleozoic–Early Mesozoic geodynamics of Central Asia. Gondwana Research 7, 791–808.
Carroll, A.R., Liang, Y., Graham, S.M., Xiao, X., Hendrix, M.S., Chu, J., McKnight, C.L., 1990. Junggar basin, northwest China: trapped Late Paleozoic ocean. Tectonophysics 181, 1–14.
Charvet, J., Laurent-Charvet', S., Shu, L., Ma, R., 2001. Paleozoic continental accretions in Central Asia around Junggar block: new structural and geochronological data. Gondwana Research 4, 590–592.
Charvet, J., Shu, S.L., Laurent-Charvet, S., 2007. Paleozoic structural and geodynamic evolution of eastern Tianshan (NW China): welding of the Tarim and Junggar plates. Episodes 30, 162–186.
Chen, B., Jahn, B.M., 2004. Genesis of post-collisional granitoids and basement nature of the Junggar Terrane, NW China: Nd–Sr isotope and trace element evidence. Journal of Asian Earth Sciences 23, 691–703.
Choulet, F., Faure, M., Cluzel, D., Chen, Y., Lin, W., Wang, B., 2012. From oblique accretion to transpression in the evolution of the Altaid collage: new insights from West Junggar, northwestern China. Gondwana Research 21, 530–547.
Coleman, R.G., 1989. Continental growth of northwest China. Tectonics 8, 621–635.
Condie, K.C., 1999. Mafic crustal xenoliths and the origin of the lower continental crust. Lithos 46, 95–101.
Corfu, F., Hanchar, J.M., Hoskin, P.W.O., Kinny, P., 2003. Atlas of zircon textures. Reviews in Mineralogy and Geochemistry 53, 469–500.
Davidson, J.P., Hora, J.M., Garrison, J.M., Dungan, M.A., 2005. Crustal forensics in arc magmas. Journal of Volcanology and Geothermal Research 140, 157–170.
Defant, M.J., Drummond, M.S., 1990. Derivation of some modern arc magmas by melting of young subducted lithosphere. Nature 347, 662–665.
DePaolo, D.J., 1981. Neodymium isotopes in the Colorado Front Range and crust–mantle evolution in the Proterozoic. Nature 291, 193–196.
Dimalanta, C., Taira, A., Yumul Jr., G.P., Tokuyama, H., Mochizuki, K., 2002. New rates of western Pacific island arc magmatism from seismic and gravity data. Earth and Planetary Science Letters 202, 105–115.
Dong, L.H., Xu, X.W., Qu, X., Li, G.M., 2009. Tectonic setting and formation mechanism of the circum-Junggar porphyritic copper deposit belts. Acta Petrologica Sinica 25, 713–717 (in Chinese with English abstract).
Du, S.J., Qu, X., Deng, G., Zhang, Y., Cheng, S.L., Lu, H.F., Wu, Q., Xu, X.W., 2010. Chronology and tectonic setting of intrusive bodies and associated porphyry copper deposit in the Hersai area, Eastern Junggar. Acta Petrologica Sinica 26, 2981–2996 (in Chinese with English abstract).
Ellam, R.M., Hawkesworth, C.J., 1988. Elemental and isotopic variations in subduction related basalts: evidence for a three component model. Contributions to Mineralogy and Petrology 98, 72–80.
Filippova, I.B., Bush, V.A., Didenko, A.N., 2001. Middle Paleozoic subduction belts: the leading factor in the formation of the Central Asian fold-and-thrust belt. Russian Journal of Earth Sciences 3, 405–426.
Gan, L., Tang, H.F., Han, Y.J., 2010. Geochronology and geochemical characteristics of the Yemaquan granitic pluton in East Junggar,Xinjiang. Acta Petrologica Sinica 26, 2374–2388 (in Chinese with English abstract).
Goldstein, S.L., O'Nions, R.K., Keith, R., Hamilton, P.J., 1984. A Sm–Nd isotopic study of atmospheric dusts and particulates from major river systems. Earth and Planetary Science Letters 70, 221–236.
Goolaerts, A., Mattielli, N., de Jong, J., Weis, D., Scoates, J.S., 2004. Hf and Lu isotopic reference values for the zircon standard 91500 by MC-ICP-MS. Chemical Geology 206, 1–9.
Gu, L.X., Hu, S.X., Yu, C.S., Li, H.Y., Xiao, X.J., Yan, Z.F., 2000. Carboniferous volcanites in the Bogda orogenic belt of eastern Tianshan and their tectonic implications. Acta Petrologica Sinica 16, 305–316.
Guillot, S., Le Fort, P., Pecher, A., Barman, M.R., Aprahamian, J., 1995. Contact metamorphism and depth of emplacement of the Manaslu granite (central Nepal): implications for Himalayan orogenesis. Tectonophysics 241, 99–119.
He, G.Q., Li, M.S., Liu, D.Q., Zhou, N.H., 1994. Palaeozoic Crustal Evolution and Mineralization in Xinjiang of China. Xinjiang People's Publication House, Urumqi, p. 437 (in Chinese with English abstract).
Hofmann, A.W., 1988. Chemical differentiation of the Earth: the relationship between mantle, continental crust and oceanic crust. Earth and Planetary Science Letters 90, 297–314.
Hofmann, A.W., Jochum, K.P., Seufert, M., White, W.M., 1986. Nb and. Pb in oceanic basalts: new constraints on mantle evolution. Earth and Planetary Science Letters 79, 33–43.
Hu, A., Wei, G.J., 2003. A review of ages of basement rocks from Junggar basin in Xinjiang, China—based on studies of geochronology. Xinjiang Geology 21, 398–406 (in Chinese with English abstract).
Hu, A., Wei, G., Deng, W., Zhang, J., Chen, L., 2006. 1.4 Ga SHRIMP U–Pb age for zircons of granodiorite and its geological significance from the eastern segment of the Tianshan Mountains, Xinjiang, China. Geochimica 35, 333–345 (in Chinese with English abstract).
Irvine, T.N., Baragar, W.R.A., 1971. A guide to the chemical classification of the common volcanic rocks. Canadian Journal of Earth Sciences 8, 523–548.
Jahn, B.M., Wu, F., Lo, C.H., Tsai, C.H., 1999. Crust–mantle interaction induced by deep subduction of the continental crust: geochemical and Sr–Nd isotopic evidence from post-collisional mafic–ultramafic intrusions of the northern Dabie complex, central China. Chemical Geology 157, 119–146.
Jakeš, P., White, A.J.R., 1971. Composition of island arcs and continental growth. Earth and Planetary Science Letters 12, 224–230.
Jian, P., Liu, D.Y., Zhang, Q., Zhang, F.Q., Shi, Y.R., Shi, G.H., Zhang, L.Q., Tao, H., 2003. SHRIMP dating of ophiolite and leucocratic rocks within ophiolite. Earth Science Frontier 10, 439–456 (in Chinese with English abstract).
Jowhar, T.N., 2001. Geobarometric constraints on the depth of emplacement of granite from the Ladakh batholith, Northwest Himalaya, India. Journal of Mineralogical and Petrological Sciences 96, 256–264.
Kearey, P., Klepeis, K.A., Vine, F., 2009. Global Tectonics, third edition. Wiley-Blackwell, John Wiley & Sons, West Sussex, UK, p. 482.
Kesler, S.E., Wilkinson, B.H., 2008. New insight into earth's mineral endowment: model-based estimation of global copper resources. Geology 36, 255–258.
Kröner, A., Windley, B.F., Badarch, G., Tomurtogoo, O., Hegner, E., Jahn, B.M., Gruschka, S., Khain, E.V., Demoux, A., Wingate, M.T.D., 2007. Accretionary growth and crust formation in the Central Asian orogenic belt and comparison with the Arabian–Nubian shield. In: Hatcher, R.D., Carlson, M.P., McBride, J.H. (Eds.), 4-D Framework of Continental Crust: Geological Society of America Memoir, 200, pp. 181–209.
Le Bas, M.J., Le Maitre, R.W., Streckeisen, A., Zanettin, B., 1986. A chemical classification of volcanic rocks based on the total alkalisilica diagram. Journal of Petrology 27, 745–750.
Leake, B.E., Woolley, A.R., Arps, C.E.S., Birch, W.D., Gilbert, M.C., Grice, J.D., Hawthorne, F.C., Kato, A., Kisch, H.J., Krivovichev, V.G., Linthout, K., Laird, J., Mandarino, J.A., Maresch, W.V., Nickel, E.H., Rock, N.M.S., Schumacher, J.C., Smith, D.C., Stephenson, N.C.N., Ungaretti, L., Whittaker, E.J.W., Youzhi, G., 1997. Nomenclature of amphiboles: report of the subcommittee on amphiboles of the International Mineralogical Association, Commission on New Minerals and Mineral Names. Mineralogical Magazine 61, 295–321.
Lehmann, J., Schulmann, K., Lexa, O., Corsini, M., Kröner, A., Štípská, P., Tomurhuu, D., Otgonbator, D., 2010. Structural constraints on the evolution of the Central Asian Orogenic Belt in SW Mongolia. American Journal of Science 310, 575–628.
Li, J.Y., Xiao, X.C., Chen, W., 2000. Late Ordovician continental basement of the eastern Junggar Basin in Xinjiang, NW China: evidence from the Laojunmiao metamorphic complex on the northeast basin margin. Xinjiang Geology 19, 297–302 (in Chinese with English abstract).
Li, X.H., Liu, Y., Li, Q.L., Guo, C.H., Chamberlain, K.R., 2009. Precise determination of Phanerozoic zircon Pb/Pb age by multi-collector SIMS without external standardization. Geochemistry, Geophysics, Geosystems 10, Q04010. http://dx.doi.org/10.1029/2009GC002400.
Li, Q.L., Li, X.H., Liu, Y., Tang, G.Q., Yang, J.H., Zhu, W.G., 2010. Precise U–Pb and Pb–Pb dating of Phanerozoic baddeleyite by SIMS with oxygen flooding technique. Journal of Analytical Atomic Spectrometry 25, 1107–1113.

Please cite this article as: Xu, X.-W., et al., Tectonic evolution of the East Junggar terrane: Evidence from the Taheir tectonic window, Xinjiang, China, Gondwana Research (2012), http://dx.doi.org/10.1016/j.gr.2012.11.007

Lin, J.F., Yu, H.X., Yu, X.Q., Di, Y.J., Tian, J.T., 2007. Zircon SHRIMP U–Pb dating and geological implication of the Sabei alkali-rich granite from Eastern Junggar of Xinjiang, NW China. Acta Petrologica Sinica 23, 1876–1884 (in Chinese with English abstract).
Liu, W., Liu, X.J., Xiao, W.J., 2012. Massive granitoid production without massive continental-crust growth in the Chinese Altay: insight into the source rock of granitoids using integrated zircon U–Pb age, Hf–Nd–Sr isotopes and geochemistry. American Journal of Science 312, 629–684. http://dx.doi.org/10.2475/06.2012.02.
Long, L., Gao, J., Klemd, R., Beier, C., Qian, Q., Zhang, X., Wang, J., Jiang, T., 2011. Geochemical and geochronological studies of granitoid rocks from the Western Tianshan Orogen: implications for continental growth in the southwestern Central Asian Orogenic Belt. Lithos 126, 321–340.
Long, X., Yuan, C., Sun, M., Safonova, I., Xiao, W., Wang, Y., 2012. Geochemistry and U–Pb detrital zircon dating of Paleozoic graywackes in East Junggar, NW China: insights into subduction–accretion processes in the southern Central Asian Orogenic Belt. Gondwana Research 21, 637–653.
Ludwig, K.R., 2001. Users' manual for Isoplot/Ex rev. 2.49. Berkeley Geochronology Centre Special Publication. No. 1a.
Macdonald, R., Hawkesworth, C.J., Heath, E., 2000. The Lesser Antilles volcanic chain: a study in arc magmatism. Earth-Science Review 49, 1–76.
Mahoney, J.J., Storey, M., Duncan, R.A., Spencer, K.J., Pringle, M., 1993. Geochemistry and geochronology of Leg 130 basement lavas: nature and origin of the Ontong-Java plateau. Proceedings of the Ocean Drilling Program, Scientific Results 130, 3–22.
Mooney, W.D., Laske, G., Masters, T.G., 1998. CRUST 5.1: a global crustal model at 5°×5°. Journal of Geophysical Research 103, 727–747.
Nelson, B.K., Depaolo, D.J., 1985. Rapid production of continental crust 1.7 to 1.9 by ago: Nd isotopic evidence from the basement of the North American mid-continent. Geological Society of America Bulletin 96, 746–754.
Othman, D.B., White, W.M., Patchett, J., 1989. The geochemistry of marine sediments, island arc magma genesis, and crust-mantle recycling. Earth and Planetary Science Letters 94, 1–21.
Pearce, J.A., 1983. Role of the sub-continental lithosphere in magma genesis at active continental margins. In: Hawkesworth, C.L., Norry, M.J. (Eds.), Continental Basalts and Mantle Xenoliths. Shiva, Nantwich, UK, pp. 230–249.
Pearce, J.A., Harris, N.B.W., Tindle, A.G., 1984. Trace element discrimination diagrams for the tectonic interpretation of granitic rocks. Journal of Petrology 25, 956–983.
Ping, J., Dunyi, L., Yuruo, S., Fuqin, Z., 2005. SHRIMP dating of SSZ ophiolites from northern Xinjiang Province, China: implications for generation of oceanic crust in the Central Asian Orogenic Belt. In: Sklyarov, E.V. (Ed.), Structural and tectonic correlation across the Central Asia orogenic collage: north-eastern segment. Guidebook and Abstract Volume of the Siberian Workshop IGCP-480. IEC SB RAS, Irkutsk, p. 246.
Plank, T., Langmuir, C.H., 1993. Tracing trace elements from sediment input to volcanic output at subduction zones. Nature 362, 739–743.
Qu, X., Xu, X.W., Liang, G.L., Qu, W.J., Du, S.J., Jiang, N., Wu, H.P., Zhang, Y., Xiao, H., Dong, L.H., 2009. Geological and geochemical characteristics of the Mengxi Cu–Mo deposit and its constrain on tectonic setting of the Qiongheba magmatic arc in eastern Junggar, Xinjiang. Acta Petrologica Sinica 25, 765–776 (in Chinese with English abstract).
RGSIXJBGMR, 2000. Geological map and explanatory text of Zhifang, Xinjiang. China Geological Survey Map L46C004002, scale 1:250,000.
RGSIXJBGMR (The regional geological survey institute of Xinjiang Bureau of Geology and Mineral Resources), 1978. Geological map and explanatory text of Hongliuxia, Xinjiang. China Geological Survey Map L-46-32, scale 1:200,000.
Seedorff, E., Dilles, J.H., Proffett, J.M., Einaudi, M.T., Zurcher, L., Stavast, W.J.A., Johnson, D.A., Barton, M.D., 2005. Porphyry deposits. Characteristics and origin of hypogene features. Economic Geology 100th. Anniverary, pp. 251–298.
Sengör, A.M.C., Natal'in, B.A., 1996. Turkic-type orogeny and its role in the making of the continental crust. Annual Review of Earth and Planetary Science Letters 24, 263–337.
Sengör, A.M.C., Natal'in, B.A., Burtman, V.S., 1993. Evolution of the Altaid tectonic collage and Paleozoic crustal growth in Eurasia. Nature 364, 299–307.
Shen, P., Shen, Y., Li, X.H., Pan, H., Zhu, H., Meng, L., Dai, H., 2012. Northwestern Junggar Basin, Xiemisitai Mountains, China: a geochemical and geochronological approach. Lithos 140–141, 103–118.
Shu, L., Wang, Y., 2003. Late Devonian–Early Carboniferous radiolarian fossils from siliceous rocks of the Kelameili Ophiolite, Xinjiang. Geological Review 49, 408–412.
Sides, J.R., 1980. Emplacement of the Butler Hill Granite, a shallow pluton within the St. Francois Mountains batholith, southeastern Missouri. Geological Society of America Bulletin 91, 535–540.
Stacey, J.S., Kramers, J.D., 1975. Approximation of terrestrial lead isotope evolution by a two-stage model. Earth and Planetary Science Letters 26, 207–221.
Steiger, R.H., Jäger, E., 1977. Subcommission on geochronology. Convention on the use of decay constants in geo- and cosmochronology. Earth and Planetary Science Letters 36, 359.
Su, Y., Tang, H., Cong, F., 2008. Zircon U–Pb age and petrogenesis of the Huangyangshan alkaline granite body in East Junggar, Xinjiang. Acta Mineralogica Sinica 28, 117–126 (in Chinese with English abstract).
Su, Y., Zheng, J., Griffin, W.L., Zhao, J., Tang, H., Ma, Q., Lin, X., 2012. Geochemistry and geochronology of Carboniferous volcanic rocks in the eastern Junggar terrane, NW China: implication for a tectonic transition. Gondwana Research 22, 1009–1029.
Sun, S.S., McDonough, W.F., 1989. Chemical and isotopic systematics of ocean basalts: implications for mantle composition and processes. In: Saunders, A.D., Norry, M.J. (Eds.), Magmatism in Ocean Basins: Geological Society, Special Publication, London, 42, pp. 313–345.
Taira, A., 2001. Tectonic evolution of the Japanese island arc system. Annual Review of Earth and Planetary Sciences 29, 109–134.
Tang, H.F., Qu, W.J., Su, Y.P., Hou, G.S., Du, A.D., Cong, F., 2007. Genetic connection of Sareshike tin deposit with the alkaline A-type granites of Sabei body in Xinjiang: constraint from isotopic ages. Acta Petrologica Sinica 23, 1989–1997 (in Chinese with English abstract).
Tera, F., Brown, L., Morris, J., Sacks, I.S., Klein, J., Middleton, R., 1986. Sediment incorporation in island-arc magmas: inferences from 10Be. Geochimica et Cosmochimica Acta 50, 535–550.
Tomiya, A., Takahashi, E., Furukawa, N., Suzuk, I.T., 2010. Depth and evolution of a silicic magma chamber: melting experiments on a low-k rhyolite from Usu Volcano, Japan. Journal of Petrology 51, 1333–1354.
Wan, B., Xiao, W.J., Zhang, L.C., Windley, B.F., Han, C.M., Quinn, C.D., 2011. Contrasting styles of mineralization in the Chinese Altai and East Junggar, NW China: implications for the accretionary history of the southern Altaids. Journal of the Geological Society 168, 1311–1321.
Wang, S., 1992. Constraints of chlorine on $^{40}Ar/^{39}Ar$ dating and calculation of high-precise $^{40}Ar/^{39}Ar$ ages. Scientia Geologica Sinica 27, 369–378 (in Chinese with English abstract).
Wang, B.Y., Li, H.H., 1989. Division and correlation of Middle and Upper Silurian in the Kelamaili Region of Xinjiang. Xinjiang Geology 7, 53–66 (in Chinese with English abstract).
Wang, S., Sang, H., Hu, S., 1985. 40Ar/39Ar age determinant using 49–2 reactor and $^{40}Ar/^{39}Ar$ age spectrum for amphibolite from Qianan, China. Acta Petrologica Sinica 2, 35–44 (in Chinese with English abstract).
Wang, F., He, H.Y., Zhu, R.X., Sang, H.Q., Wang, Y.L., Yang, L.K., 2005. Intercalibration of international and domestic $^{40}Ar/^{39}Ar$ dating standards. Science in China (Series D) 35, 617–626.
Wang, F., He, H.Y., Zhu, R.X., Yang, L.K., Sang, H.Q., Wang, Y.L., 2006. Laser step-heating $^{40}Ar/^{39}Ar$ dating on young volcanic rocks. Chinese Science Bulletin 51, 2892–2896.
Watson, M.P., Hayward, A.B., Parkinson, D.M., Zhang, Z.M., 1987. Plate tectonic history, basin development and petroleum source rock deposition onshore China. Marine and Petroleum Geology 4, 205–255.
Wiedenbeck, M., Alle, P., Corfu, F., Griffin, W.L., Meier, M., Oberli, F., Vonquadt, A., Roddick, J.C., Speigel, W., 1995. Three natural zircon standards for U–Th–Pb, Lu–Hf, trace-element and REE analyses. Geostandard Newsletter 19, 1–23.
Wilson, J.T., 1966. Did the Atlantic close and then re-open? Nature 211, 676–681.
Windley, B.F., Kröner, A., Guo, J., Qu, G., Li, Y., Zhang, C., 2002. Neoproterozoic to Paleozoic geology of the Altai orogen, NW China: new zircon age data and tectonic evolution. Journal of Geology 110, 719–739.
Winter, J.D., 2001. An Introduction to Igneous and Metamorphic Petrology. Prentice Hall, pp. 150–210.
Windley, B.F., Alexeiev, D., Xiao, W.J., Kröner, A., Badarch, G., 2007. Tectonic models for accretion of the Central Asian Orogenic Belt. Journal of the Geological Society of London 164, 31–47.
Wong, K., Sun, M., Zhao, G., Yuan, C., Xiao, W., 2010. Geochemical and geochronological studies of the Alegedayi Ophiolitic Complex and its implication for the evolution of the Chinese Altai. Gondwana Research 18, 438–454.
Woodhead, J., Hergt, J., Shelley, M., Eggins, S., Kemp, R., 2004. Zircon Hf-isotope analysis with an excimer laser, depth profiling, ablation of complex geometries, and concomitant age estimation. Chemical Geology 209, 121–135.
Wu, B., He, G.Q., Wu, T.R., Li, H.J., Luo, H.L., 2006a. Discovery of the Buergen ophiolitic me′lange belt in Xinjiang and its tectonic significance. Geology in China 33, 476–486 (in Chinese with English abstract).
Wu, F.Y., Yang, Y.H., Xie, L.W., Yang, J.H., Xu, P., 2006b. Hf isotopic compositions of the standard zircons and baddeleyites used in U–Pb geochronology. Chemical Geology 234, 105–126.
Wu, Q., Qu, X., Zhang, Y., Dong, L.H., Xu, X.W., 2012. Geochronology of Hongliuxia ductile shear zone and its constraint on the closure of the Junggar Ocean. Acta Petrologica Sinica 28, 2331–2339 (in Chinese with English abstract).
XBGMR (Bureau of Geology and Mineral Resources of Xinjiang Autonomous Region), 1993. Regional Geology of Xinjiang Autonomous Region. Geological Publishing House, p. 841.
Xiang, P., Zhang, L.C., Wu, H.Y., Zhang, X.J., Chen, Z.G., Wan, B., 2009. Ages of the zircons from ore-bearing porphyries in II–III ore area of Kalaxianger porphyry copper ore belt in Qinghe, Xinjiang and its geological significance. Acta Petrologica Sinica 25, 1474–1483 (in Chinese with English abstract).
Xiao, X.C., Tang, Y.Q., Feng, Y.M., Zhu, B.Q., Li, J.Y., Zhou, M., 1992. Tectonics in Northern Xinjiang and Its Neighboring Areas. Geological Publishing House, Beijing, p. 126 (in Chinese).
Xiao, W.J., Windley, B.F., Badarch, G., Sun, S., Li, J.L., Qin, K.Z., Wang, Z.H., 2004a. Palaeozoic accretionary and convergent tectonics of the southern Altaids: implications for the lateral growth of Central Asia. Journal of the Geological Society of London 161, 339–342.
Xiao, W.J., Zhang, L.C., Qin, K.Z., Sun, S., Li, J.L., 2004b. Paleozoic accretionary and collisional tectonics of the Eastern Tianshan (China): implications for the continental growth of central Asia. American Journal of Science 304, 370–395.
Xiao, W.J., Windley, B.F., Yan, Q.R., Qin, K.Z., Chen, H.L., Yuan, C., Sun, M., Li, J.L., Sun, S., 2006. SHRIMP zircon age of the Aermantai ophiolite in the North Xinjiang, China and its tectonic implications. Acta Geologica Sinica 80, 32–36.
Xiao, W.J., Han, C.M., Yuan, C., Sun, M., Lin, S.F., Chen, H.L., Li, Z.L., Li, J.L., Sun, S., 2008. Middle Cambrian to Permian subduction-related accretionary orogenesis of Northern Xinjiang, NW China: implications for the tectonic evolution of central Asia. Journal of Asian Earth Sciences 32, 102–117.
Xiao, W.J., Windley, B.F., Yuan, C., Sun, M., Han, C.M., Lin, S.F., Chen, H.L., Yan, Q.R., Liu, D.Y., Qin, K.Z., Li, J.L., Sun, S., 2009. Paleozoic multiple subduction–accretion processes of the southern Altaids. American Journal of Science 309, 221–270.

Please cite this article as: Xu, X.-W., et al., Tectonic evolution of the East Junggar terrane: Evidence from the Taheir tectonic window, Xinjiang, China, Gondwana Research (2012), http://dx.doi.org/10.1016/j.gr.2012.11.007

Xiao, W.J., Huang, B., Han, C., Sun, S., Li, J., 2010a. A review of the western part of the Altaids: a key to understanding the architecture of accretionary orogens. Gondwana Research 18, 253–273.
Xiao, W.J., Mao, Q.G., Windley, B.F., Han, C.M., Qu, J.F., Zhang, J.E., Ao, S.J., Guo, Q.Q., Clevenn, R., Lin, S.F., Shan, Y.H., LI, J.L., 2010b. Paleozoic multiple accretionary and collisional processes of the Beishan orogenic collage. American Journal of Science 310, 1553–1594.
Xiao, Y., Zhang, H., Shi, J., Su, B., Sakyi, P.A., Lu, X., Hu, Y., Zhang, Z., 2011. Late Paleozoic magmatic record of East Junggar, NW China and its significance: implication from zircon U–Pb dating and Hf isotope. Gondwana Research 20, 532–542.
Xiao, W.J., Windley, B.F., Allen, M.B., Han, C., 2012. Paleozoic multiple accretionary and collisional tectonics of the Chinese Tianshan orogenic collage. Gondwana Research 22. http://dx.doi.org/10.1016/j.gr.2012.01.012.
Xu, X.W., Ma, T.L., 2004. Reply to the comment by Wen-Bin Zhu et al. on "Characteristics and dynamic origin of the large-scale Jiaoluotage ductile compressional zone in the eastern Tianshan Mountains, China". Journal of Structural Geology 26, 2337–2340.
Xu, X.W., Ma, T.L., Sun, L.Q., Cai, X.P., 2003. Characteristics and dynamic origin of a macro-scale ductile compressed zone formed in a Carboniferous back-arc basin, Jiaoluotage, Eastern Tianshan Mts., China. Journal of Structural Geology 25, 1901–1915.
Xu, P., Wu, F.Y., Xie, L.W., Yang, Y.H., 2004. Hf isotopic compositions of the standard zircons for U–Pb dating. Chinese Science Bulletin 49, 1642–1648.
Xu, X.W., Jiang, N., Yang, K., Zhang, B.L., Liang, G.H., Mao, Q., Li, J.X., Du, S.J., Ma, Y.G., Zhang, Y., Qin, K.Z., 2009. Accumulated phenocrysts and origin of feldspar porphyry in the Chanho area, western Yunnan, China. Lithos 113, 595–611.
Yamaji, A., 1990. Rapid intra-arc rifting in Miocene northeast Japan. Tectonics 9, 365–378.
Yang, J.H., Wu, F.Y., Chung, S.L., Chu, M.F., Wilde, S.A., 2004. Multiple sources for the origin of granites: geochemical and Nd/Sr isotopic evidence from the Gudaoling granite and its mafic enclaves, northeast China. Geochimica et Cosmochimica Acta 68, 4469–4483.
Yang, J.H., Wu, F.Y., Chung, S.L., Wilde, S.A., Chu, M.F., 2006. A hybrid origin for the Qianshan A-type granite, northeast China: geochemical and Sr–Nd–Hf isotopic evidence. Lithos 89, 89–106.
Yang, G., Li, Y., Wu, H., Zhong, X., Yang, B., Yan, C., Yan, J., Si, G., 2011. Geochronological and geochemical constrains on petrogenesis of the Huangyangshan A-type granite from the East Junggar, Xinjiang, NW China. Journal of Asian Earth Sciences 40, 722–736.
Yang, X.F., He, D.F., Wang, Q.C., Tang, Y., Tao, H.F., Li, D., 2012. Provenance and tectonic setting of the Carboniferous sedimentary rocks of the East Junggar Basin, China: evidence from geochemistry and U–Pb zircon geochronology. Gondwana Research 22, 567–584.
Zhang, Z.X., Rong, J.Y., Di, Q.L., 1983. Silurian Tuvaella giganteaFaunule (Brachiopoda) of the Barkol Area, Northeastern Xinjiang. Acta Palaeontologica Sinica 22, 278–294 (in Chinese with English abstract).
Zhang, Z.M., Liou, J.G., Coleman, R.G., 1984. An outline of the plate tectonics of China. Geological Society of America Bulletin 95, 295–312.
Zhang, C., Zhai, M., Allen, M.B., Saunders, A.D., Wang, G.R., Huang, X., 1993. Implications of Palaeozoic ophiolites from Western Junggar, NW China, for the tectonics of central Asia. Journal of the Geological Society of London 150, 551–561.
Zhang, H.X., Niu, H.C., Terada, K., Yu, X.Y., Sato, H., Ito, J., 2003. Zircon SHRIMP U–Pb dating on plagiogranite from the Kuerti ophiolite in Altay, North Xinjiang. Chinese Science Bulletin 48, 2231–2235.
Zhang, H.Y., Niu, H.C., Sato, H., Shan, Q., Yu, X.Y., Ito, J., Zhang, Q., 2004. Late Paleozoic adakite and Nb-enriched basalt from Northern Xinjiang: evidence for the southward Subduction of the Paleo-Asian Ocean. Geological Journal of China Universities 10, 106–113 (in Chinese with English abstract).
Zhang, Z.C., Yan, S.H., Chen, B.L., Zhou, G., He, Y.K., Chai, F.M., He, L.X., Wan, Y.S., 2006. SHRIMP zircon U–Pb dating for subduction-related granitic rocks in the northern part of east Junggar, Xinjiang. Chinese Science Bulletin 51, 952–962.
Zhang, Z.C., Zhou, G., Kusky, T.M., Yan, S.H., Chen, B.L., Zhao, L., 2009. Late Paleozoic volcanic record of the Eastern Junggar terrane, Xinjiang, Northwestern China: major and trace element characteristics, Sr–Nd isotopic systematics and implications for tectonic evolution. Gondwana Research 16, 201–215.
Zhang, Z., Deng, Y., Chen, L., Wu, J., Teng, J., Panza, G., 2012. Seismic structure and rheology of the crust under mainland China. Gondwana Research 22. http://dx.doi.org/10.1016/j.gr.2012.07.010.
Zhao, J., Liu, G., Lu, Z., Zhang, X., Zhao, G., 2003. Lithospheric structure and dynamic processes of the Tianshan orogenic belt and the Junggar basin. Tectonophysics 376, 199–239.
Zheng, J.P., Sun, M., Zhao, G.C., Robinson, P.T., Wan, F.Z., 2007. Elemental and Sr–Nd–Pb isotopic geochemistry of Late Paleozoic volcanic rocks beneath the Junggar basin, NW China: Implications for the formation and evolution of the basin basement. Journal of Asian Earth Sciences 29, 778–794.
Zonenshain, L., Kuzmin, M.I., Natapov, L.M., 1990. Geology of the U.S.S.R.: a plate tectonic synthesis. American Geophysical Union. Geodynamics Series 21, 1–242.

Please cite this article as: Xu, X.-W., et al., Tectonic evolution of the East Junggar terrane: Evidence from the Taheir tectonic window, Xinjiang, China, Gondwana Research (2012), http://dx.doi.org/10.1016/j.gr.2012.11.007